


# CRISPR/Cas9 Genome Editing of the Human Topoisomerase II $\alpha$ Intron 19 5' Splice Site Circumvents Etoposide Resistance in Human Leukemia K562 Cells

Victor A. Hernandez, Jessika Carvajal-Moreno, Jonathan L. Papa, Nicholas Shkolnikov, Junan Li, Hatice Gulcin Ozer, Jack C. Yalowich, and  Terry S. Elton

*Division of Pharmaceutics and Pharmacology, College of Pharmacy (V.A.H., J.C.-M., J.L.P., J.L., J.C.Y., T.S.E.) and Department of Biomedical Informatics, College of Medicine (H.G.O), The Ohio State University, Columbus, Ohio*

Received October 2, 2020; accepted December 28, 2020

## ABSTRACT

An essential function of DNA topoisomerase II $\alpha$  (TOP2 $\alpha$ ; 170 kDa, TOP2 $\alpha$ /170) is to resolve DNA topologic entanglements during chromosome disjunction by introducing transient DNA double-stranded breaks. TOP2 $\alpha$ /170 is an important target for DNA damage-stabilizing anticancer drugs, whose clinical efficacy is compromised by drug resistance often associated with decreased TOP2 $\alpha$ /170 expression. We recently demonstrated that an etoposide-resistant K562 clonal subline, KVP.5, with reduced levels of TOP2 $\alpha$ /170, expresses high levels of a novel C-terminal truncated TOP2 $\alpha$  isoform (90 kDa, TOP2 $\alpha$ /90). TOP2 $\alpha$ /90, the translation product of a TOP2 $\alpha$  mRNA that retains a processed intron 19 (I19), heterodimerizes with TOP2 $\alpha$ /170 and is a resistance determinant through a dominant-negative effect on drug activity. We hypothesized that genome editing to enhance I19 removal would provide a tractable strategy to circumvent acquired TOP2 $\alpha$ -mediated drug resistance. To enhance I19 removal in KVP.5 cells, CRISPR/Cas9 was used to make changes (GAG//GTAAAC→GAG//GTAAGT) in the TOP2 $\alpha$  gene's suboptimal exon 19/intron 19 5' splice site (E19/I19 5' SS). Gene-edited clones were identified by

quantitative polymerase chain reaction and verified by sequencing. Characterization of a clone with all TOP2 $\alpha$  alleles edited revealed improved I19 removal, decreased TOP2 $\alpha$ /90 protein, and increased TOP2 $\alpha$ /170 protein. Sensitivity to etoposide-induced DNA damage ( $\gamma$ H2AX, Comet assays) and growth inhibition was restored to levels comparable to those in parental K562 cells. Together, the results indicate that our gene-editing strategy for optimizing the TOP2 $\alpha$  E19/I19 5' SS in KVP.5 cells circumvents resistance to etoposide and other TOP2 $\alpha$ -targeted drugs.

## SIGNIFICANCE STATEMENT

Results presented here indicate that CRISPR/Cas9 gene editing of a suboptimal exon 19/intron 19 5' splice site in the DNA topoisomerase II $\alpha$  (TOP2 $\alpha$ ) gene results in circumvention of acquired drug resistance to etoposide and other TOP2 $\alpha$ -targeted drugs in a clonal K562 cell line by enhancing removal of intron 19 and thereby decreasing formation of a truncated TOP2 $\alpha$  90 kDa isoform and increasing expression of full-length TOP2 $\alpha$  170 kDa in these resistant cells. Results demonstrate the importance of RNA processing in acquired drug resistance to TOP2 $\alpha$ -targeted drugs.

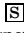
## Introduction

The human DNA topoisomerase II (TOP2 $\alpha$ ; 170 kDa, TOP2 $\alpha$ /170) enzyme functions as a homodimer to resolve DNA topology by introducing transient DNA double-stranded breaks (DSBs) essential for chromosomal segregation during mitosis (Deweese and Osheroff, 2009; Nitiss, 2009). TOP2 $\alpha$ /170 enzymatic activity is necessary for cell survival and is highly expressed in rapidly

proliferating cells. This has made TOP2 $\alpha$ /170 an important target in cancer therapy (Chen et al., 2013; Pommier et al., 2016). Type IIA topoisomerase interfacial inhibitors, such as etoposide, stabilize the enzyme-DNA complexes by insertion within the break sites generated by TOP2 $\alpha$ /170, thereby inhibiting religation, resulting in DSBs and triggering cell death (Pommier and Marchand, 2011).

Resistance to TOP2 $\alpha$  interfacial poisons is frequently associated with a reduction of TOP2 $\alpha$ /170 expression levels or its altered subcellular localization (Ganapathi and Ganapathi, 2013; Capelôa et al., 2020). We previously demonstrated that acquired resistance to etoposide in a human K562 leukemia cell

This work was supported by National Institutes of Health National Cancer Institute [Grant R01 CA226906-01A1] (to J.C.Y. and T.S.E.)  
<https://doi.org/10.1124/molpharm.120.000173>

 This article has supplemental material available at [molpharm.aspetjournals.org](https://molpharm.aspetjournals.org).

**ABBREVIATIONS:** AML, acute myeloid leukemia; bp, base pair; Cas9, CRISPR-associated protein 9; CCTop, CRISPR/Cas9 Target Online Predictor; CI, confidence interval; CMV pro, cytomegalovirus promoter; crRNA, CRISPR RNA; DMEM, Dulbecco's modified Eagle's medium; DSB, double-stranded break; E19, exon 19; E20, exon 20; GAPDH, glyceraldehyde-3-phosphate dehydrogenase; GCD, genomic cleavage detection; gRNA, crRNA:tracrRNA duplex;  $\gamma$ H2AX, phosphorylated Ser-139 residue of the H2A histone family member X; HDR, homology-directed repair; HPRT1, hypoxanthine-guanine phosphoribosyltransferase; I19, intron 19; indel, insertions/deletion; NHEJ, nonhomologous end joining; PAM, protospacer-adjacent motif; PCR, polymerase chain reaction; polyA site, polyadenylation site; qPCR, quantitative PCR; RNA-seq, RNA sequencing; SS, splice site; ssODN, single-stranded oligo DNA nucleotide; TOP2 $\alpha$ , DNA topoisomerase II $\alpha$  protein; TOP2 $\alpha$ /170, TOP2 $\alpha$  170 kDa; TOP2 $\alpha$ /90, TOP2 $\alpha$  90 kDa; T7 pro, T7 polymerase promoter; tracrRNA, *trans*-activating CRISPR RNA.

line, K/VP.5, is associated with decreased TOP2 $\alpha$ /170 mRNA/protein expression levels and a dramatically increased expression of a novel TOP2 $\alpha$  mRNA (University of California Santa Cruz Genome Browser accession number MH936673), which retains a processed intron 19 (I19) and encodes a 90-kDa TOP2 $\alpha$  isoform now designated TOP2 $\alpha$ /90 (Kanagasabai et al., 2017; Elton et al., 2020). Importantly, the TOP2 $\alpha$ /90 isoform heterodimerizes with TOP2 $\alpha$ /170, resulting in a dominant-negative effect with respect to etoposide-induced covalent TOP2 $\alpha$ -DNA complexes, DNA damage, and cytotoxicity (Kanagasabai et al., 2018), thereby functioning as a resistance determinant.

Over 95% of genes undergo alternative pre-mRNA splicing, a process by which a single pre-mRNA is matured into multiple mRNA isoforms (Lee and Rio, 2015). This leads to the expression of different mRNA isoforms and is responsible for proteomic diversity. Several types of alternative splicing of a pre-mRNA have been described, including intron retention (Lee and Rio, 2015). Although most intron-retaining mRNA transcripts are susceptible to nuclear intron detention (Boutz et al., 2015) or nonsense-mediated decay (Kurosaki and Maquat 2016), some intron-retaining transcripts leave the nucleus and undergo translation to produce new protein isoforms with novel functions (Li et al., 2016; Uzor et al., 2018; Shoubridge et al., 2019; Wang et al., 2019b). This process seems to occur in a number of TOP2 $\alpha$  intron-retaining mRNA variants that are translated into novel truncated TOP2 $\alpha$  isoforms and play a role in chemoresistance (Harker et al., 1995; Yu et al., 1997; Mo and Beck, 1997; Kanagasabai et al., 2017, 2018; Elton et al., 2020).

Intron retention is regulated by a complex combination of *cis*- and *trans*-acting factors (Monteuuis et al., 2019). One *cis*-acting sequence feature is the presence of weak or suboptimal splice site (SS) at the 5' and/or 3' ends of the intron, which can impede the spliceosome's ability to recognize introns that should be spliced out (Hicks et al., 2010; Huang et al., 2012; Eckert et al., 2016). Studies investigating intron retention events have demonstrated that removal of retained introns could be enhanced by strengthening the suboptimal 5' SS by mutation in a minigene system (Wickramasinghe et al., 2015) or by CRISPR/CRISPR-associated protein 9 (Cas9) gene editing (Yue and Ogawa, 2018).

Since weak splice sites are inefficiently recognized by the spliceosome, which, in part, can lead to intron retention (Monteuuis et al., 2019), the human TOP2 $\alpha$  gene was subjected to SS analyses (Splice Site Score Calculation; [http://rulai.cshl.edu/new\\_alt\\_exon\\_db2/HTML/score.html](http://rulai.cshl.edu/new_alt_exon_db2/HTML/score.html)). This analysis revealed that the TOP2 $\alpha$  exon 19 (E19/I19 5' SS (GAG//GTAAAC) is suboptimal, with a score of 6.1 out of a maximum score of 12.4 for the optimal consensus 5' SS (CAG//GTAAGT). Hence, we hypothesized that this weak SS influences I19 retention and that by mutating/gene editing the TOP2 $\alpha$  E19/I19 5' SS in etoposide-resistant K/VP.5 cells, sensitivity to etoposide would be restored.

Transfection experiments utilizing a TOP2 $\alpha$ /Minigene (i.e., a plasmid that harbors a TOP2 $\alpha$  gene segment encompassing E19 through exon 20 [E20]) demonstrated that mutating the suboptimal wild-type E19/I19 5' SS (GAG//GTAAAC) to a consensus 5' SS (CAG//GTAAGT) decreased I19 retention in K/VP.5 cells, providing "proof of concept" for CRISPR/Cas9 editing as a viable strategy to circumvent resistance. Therefore, the CRISPR/Cas9 system with homology-directed repair

(HDR) (Jinek et al., 2012; Mali et al., 2013; Liang et al., 2017) was used to introduce specific gene edits (GAG//GTAAAC  $\rightarrow$  GAG//GTAAGT) in the suboptimal TOP2 $\alpha$  E19/I19 5' SS in K/VP.5 cells. Notably, in K/VP.5 edited cells, intron 19 retention was attenuated, resulting in decreased formation of TOP2 $\alpha$ /90, restoration of full-length TOP2 $\alpha$ /170 levels, and increased etoposide-induced DNA damage and growth inhibitory effects comparable to those seen in parental K562 cells. Together, these results demonstrate that CRISPR/Cas9 editing of the TOP2 $\alpha$  gene circumvents acquired drug resistance to etoposide and other TOP2 $\alpha$ -targeted drugs.

## Materials and Methods

**Cell Culture and Acute Myeloid Leukemia Blasts.** Human K562 leukemia cells were maintained in Dulbecco's modified Eagle's medium (DMEM) (Corning, Manassas, VA) supplemented with 10% FBS. Etoposide-resistant K/VP.5 cells were selected and cloned subsequent to intermittent and eventually continuous exposure of K562 cells to 0.5  $\mu$ M etoposide as previously described (Ritke and Yalowich, 1993). K/VP.5 and gene-edited clonal cells were maintained in DMEM/10% FBS with etoposide (0.5  $\mu$ M) added every other week. CRISPR clones, generated from K/VP.5 cells, were maintained in DMEM/10% FBS. All experiments described below were performed utilizing cells growing in log phase. Deidentified blast cells from patients newly diagnosed with acute myeloid leukemia (AML) and from the same patients at relapse (who previously received TOP2 $\alpha$ -targeted therapies) were obtained from The Ohio State University Comprehensive Cancer Center Leukemia Tissue Bank Shared Resource.

**Human TOP2 $\alpha$ /170 and TOP2 $\alpha$ /90 Real-Time Polymerase Chain Reaction Assays.** Total RNA was isolated from K562, K/VP.5, CRISPR/Cas9-edited K/VP.5 cells, and blasts from patients with AML (matched pretreatment and relapse) using the RNA Easy Plus Mini Kit (cat. no. 74134; Qiagen, Germantown, MD). To ensure complete removal of contaminating DNA, an on-column digestion of DNA with RNase-free DNase (cat. no. 79254; Qiagen) was included during RNA purification. RNA (1  $\mu$ g) was reverse transcribed using random hexamers and MultiScribe Reverse Transcriptase (High Capacity cDNA Reverse Transcription Kit, cat. no. 4368814; ThermoFisher Scientific, Waltham, MA) as previously described by our laboratory (Kanagasabai et al., 2017, 2018). Quantitative real-time polymerase chain reaction (PCR) experiments (total reaction volume 10  $\mu$ l) were performed in duplicate using TaqMan Gene Expression hydrolysis probes (ThermoFisher Scientific) as previously described (Kanagasabai et al., 2017, 2018). TOP2 $\alpha$ /170 mRNA expression levels were measured using a hydrolysis probe spanning the TOP2 $\alpha$  E19/E20 boundary (5'-TCATGGTGAGATGTCACTAATGATG-3') (TaqMan assay Hs01032135\_m1), specific for TOP2 $\alpha$ /170 cDNAs. TOP2 $\alpha$ /90 mRNA expression levels were measured using a custom hydrolysis probe that spans the wild-type E19/I19 boundary (5'-TCATGGTGAGGTAAACACACAATCC-3'). A custom hydrolysis probe was also synthesized that harbored CRISPR/Cas9-mediated changes (bolded and underlined below) in the E19/I19 boundary (5'-TCATG**C**TGAGG**TAAAGT**ACACAATCC-3') to specifically measure the expression levels of edited TOP2 $\alpha$ /90 mRNAs transcribed in the K/VP.5/edit-3 cell line. Finally, a custom hydrolysis probe was synthesized that harbored the CRISPR/Cas9-mediated change (bolded and underlined) in the E19/E20 boundary (5'-TCATG**C**TGAGATG**TAAGT**ACTAATGATG-3') to specifically measure the expression levels of edited TOP2 $\alpha$ /170 mRNAs transcribed in the K/VP.5/edit-3 cell line. The relative mRNA expression levels of TOP2 $\alpha$ /90, edited TOP2 $\alpha$ /90, TOP2 $\alpha$ /170, and edited TOP2 $\alpha$ /170 in each cell line were normalized to TATA-binding protein (TaqMan assay Hs9999910\_m1) expression using the  $2^{-\Delta\Delta Ct}$  method (Schmittgen and Livak, 2008).

**Immunoassays.** K562, K/VP.5, and CRISPR/Cas9-edited K/VP.5 (with or without etoposide treatment) cellular extracts were subjected

to Western blot analysis as previously described (Kanagasabai et al., 2017, 2018). Unless otherwise noted, 16  $\mu\text{g}$  of protein was loaded into each well. Membranes were incubated overnight at 4°C with one of the following primary antibodies: a rabbit polyclonal antibody raised against the human TOP2 $\alpha$ /90/170 N-terminal sequence (amino acids 14–27) (cat. no. ab74715; used at 1:1000 dilution; Abcam, Cambridge, MA), a mouse monoclonal glyceraldehyde-3-phosphate dehydrogenase (GAPDH) antibody (cat. no. sc-47724; used at 1:5000 dilution; Santa Cruz Biotechnology, Santa Cruz, CA), a mouse phosphorylated Ser-139 residue of the H2A histone family member X ( $\gamma$ H2AX) monoclonal antibody (cat. no. sc-25330; used at 1:500 dilution; Santa Cruz Biotechnology). The membranes were subsequently incubated at room temperature for ~3 hours with a donkey anti-rabbit or anti-mouse secondary antibody (1:5000 dilution) (Jackson Immuno Research, West Grove, PA). Finally, TOP2 $\alpha$  isoforms, GAPDH, and  $\gamma$ H2AX were detected using the Immun-Star or Clarity Max chemiluminescence kits (Bio-Rad Laboratories, Hercules, CA). All immunoassay images were acquired with the ChemiDoc XRS+ imaging system and analyzed with ImageLab software (Bio-Rad Laboratories).

**TOP2 $\alpha$ /Minigene Constructs.** The pDNA3.1(+) mammalian expression plasmid (ThermoFisher Scientific) was linearized by NheI/XbaI digestion in CutSmart buffer according to the manufacturer's protocol (New England Biolabs, Ipswich, MA). Using human genomic DNA as a template, a 1355–base pair (bp) fragment encompassing the TOP2 $\alpha$  gene from just inside the beginning of E19 through E20 was PCR amplified by utilizing sense (5'-CCCAA GCTGGCTAGCGTCAGAGAAAGGTTTTGTTACT-3') and antisense (5'-CCCTCTAGACTCGAGCTGAGCATTGTAAGATGTA TCG-3') primers employing standard PCR procedures with a proof-reading polymerase, CloneAmp HiFi (cat. no. 639298; Takara Bio Inc., Kusatsu, Shiga, Japan). The primer sequences homologous to the regions just downstream of the beginning of TOP2 $\alpha$  E19 and immediately upstream of the end of TOP2 $\alpha$  E20 are bolded. The sense and antisense primers also harbor 15-nucleotide extensions (not bolded) that are homologous to ends of the NheI/XbaI linearized pCR3.1 plasmid and are necessary for "In-Fusion" cloning methodology (In-Fusion HD Cloning Kit, cat. no. 638916; Takara Bio Inc.). The TOP2 $\alpha$  E19/I19/E20 amplicon was gel purified and subcloned into the NheI/XbaI linearized pCR3.1 plasmid according to the manufacturer's protocol. The authenticity and orientation of the inserts relative to the cytomegalovirus promoter were confirmed by dideoxy sequencing. The resulting recombinant pCR/TOP2 $\alpha$ /E19/I19/E20 "minigene" plasmid was designated TOP2 $\alpha$ /Minigene1.

The suboptimal wild-type E19/I19 5' SS (GAG/GTAAAC) harbored in the TOP2 $\alpha$ /Minigene1 plasmid was mutated to a consensus 5' SS (CAG/GTAAAGT) using a Q5 Site-Directed Mutagenesis kit (cat. no. E0554S; New England Biolabs) following the manufacturer's instructions. The primers used for mutagenesis were sense (5'-CAGGTAA GTACACAATCCATGAAACC-3') and antisense (5'-ACCATGATG ATAAGAAGACATTTTCAGC-3'). Importantly, these primers were designed with their 5' ends annealing back-to-back (inverse PCR). The nucleotides that were mutated are shown in bold print and were confirmed by dideoxy sequencing. The mutated consensus E19/I19 5' SS plasmid was designated TOP2 $\alpha$ /Minigene2.

**Transfection and TOP2 $\alpha$ /Minigene1/2 PCR Amplification.** K562 and K/VP.5 cells ( $2.25 \times 10^6$  cells in 100  $\mu\text{l}$  per condition) were transfected with TOP2 $\alpha$ /Minigene1 or TOP2 $\alpha$ /Minigene2 (5.0  $\mu\text{g}$  plasmid) by electroporation technology (Nucleofector Kit V; Lonza, Basel, Switzerland), according to the manufacturer's instructions. Twenty-four hours after transfection, total RNA was isolated from transfected K562 and K/VP.5 cells and reverse transcribed as described above. The cDNA was subsequently PCR amplified using a T7 forward primer (5'-CGAAATTAATACGACTACTATAGG-3') and a TOP2 $\alpha$  I19 reverse primer (5'-GCAGACTTATGAATATCCCTGCAG G-3') or a TOP2 $\alpha$  E20 reverse primer (5'-GCAAGAGTTTATGATTAT TGCTACC-3') using AmpliTaq DNA Polymerase (cat. no. N8080160; ThermoFisher). PCR products were fractionated by electrophoresis on a 1.5% agarose gel, and PCR amplicons were visualized under UV light

after staining with 0.5 mg/ml ethidium bromide. Images were captured using the ChemiDoc XRS1 imaging system and analyzed using ImageLab software (Bio-Rad Laboratories).

**Genomic Cleavage Detection.** TrueGuide hypoxanthine-guanine phosphoribosyltransferase (HPRT1) positive control CRISPR RNA (crRNA) (5'-GCAUUUCAGUCCUAAACA-3') (cat. no. A35517), custom TrueGuide TOP2 $\alpha$  crRNA #1 (5'-GTCTTCTTATCATCATGG TG-3'), TrueGuide TOP2 $\alpha$  crRNA #2 (5'-GAAATGTCTTCTTATCAT CA-3'), TrueGuide TOP2 $\alpha$  crRNA #3 (5'-TATAATGCTTTCTGGAAA CA-3'), and TrueGuide 72-bp *trans*-activating CRISPR RNA (tracrRNA) (cat. no. A35517) were obtained from ThermoFisher. Each TrueGuide RNA is chemically modified (2'-O-methyl analogs and phosphorothioate linkages) to increase editing efficiency and protect against nuclease degradation. All TrueGuide crRNAs were individually annealed to a common tracrRNA scaffold according to the manufacturer's instructions for a final crRNA:tracrRNA duplex (gRNA) concentration of 20  $\mu\text{M}$ . The gRNAs (0.5  $\mu\text{g}$ ) were individually incubated with 2  $\mu\text{g}$  TrueCut Cas9 Protein v2 (cat. no. A36498; ThermoFisher) for 15 minutes to form Cas9 protein/gRNA ribonucleoprotein complexes. These complexes were subsequently transfected into etoposide-resistant K/VP.5 cells by electroporation technology (Nucleofector Kit V; Lonza, Basel, Switzerland) according to the manufacturer's instructions and as reported previously (Kanagasabai et al., 2017).

To determine if the gene-specific Cas9 protein/gRNA ribonucleoprotein complexes created on-target DSBs within the TOP2 $\alpha$  E19/I19 boundary sequence, K/VP.5 cells ( $2 \times 10^6$ ) were lysed 48 hours after transfection using cell lysis buffer/Proteinase K (GeneArt Genomic Cleavage Detection (GCD) Kit (cat. no. A24372; ThermoFisher). Genomic DNA (1  $\mu\text{l}$  of lysate) at the TOP2 $\alpha$  locus between E18 and I19 was then PCR amplified (50  $\mu\text{l}$  reaction volume) using the following primers: GCD TOP2 $\alpha$  E18 forward (5'-GATCTATCCCTT CTATGGTGG-3') and GCD TOP2 $\alpha$  I19 reverse (5'-CAGAAATCA AAGGGCAAGCAG-3'). Positive control PCR experiments were also performed at the HPRT1 intron 2 locus using the following primers: GCD HPRT1 forward (5'-AGAGGAGGGCCTTACTAA TTAC-3') and GCD HPRT1 reverse 5'-CATGCATAGCCAGTG CTTGAG-3'). The PCR amplicons were subsequently denatured, reannealed, and incubated with T7 endonuclease I (i.e., structure-selective enzyme that recognizes and cleaves mismatched DNA) to detect insertions/deletions (indels) created by nonhomologous end joining (NHEJ). The digested and nondigested PCR products were fractionated by electrophoresis on a 2% agarose gel, and images were captured as described above. The following equation was used to calculate the cleavage efficiency of HPRT1 and TOP2 $\alpha$  gRNA/Cas9: cleavage efficiency =  $\{1 - [(1 - \text{fraction cleaved})^{1/2}]\} \times 100$ , where fraction cleaved = (sum of cleaved band intensities)/(sum of the cleaved and parental band intensities).

**Genome Editing of the TOP2 $\alpha$  E19/I19 5' SS.** The suboptimal TOP2 $\alpha$  E19/I19 5' SS (GAG/GTAAAC; splicing score, 6.1) was gene-edited (GAG/GTAAAGT; splicing score, 11.6) utilizing the TOP2 $\alpha$  crRNA #2:tracrRNA duplex (gRNA-2) (see above), TrueCut Cas9 Protein, and a 180-nucleotide symmetric single-stranded oligonucleotide repair template (Ultrasmer Oligo; Integrated DNA Technologies, Coralville, Iowa; see Supplemental Table 1 for complete sequence) designated Enhanced E19/I19 5' SS/No PAM-2. This repair template equally spans TOP2 $\alpha$  E19/I19 and harbors the desired two 5' SS nucleotide changes. Moreover, this repair template harbors an additional nucleotide change to eliminate the protospacer-adjacent motif (#2 (PAM-2; see Fig. 5) to avoid recutting of edited alleles upon the repeated transfections necessary to edit all three TOP2 $\alpha$  alleles present in the clonal K562 cell line, K/VP.5 (Cioe et al., 1981; Zhou et al., 2019), at the E19/I19 5' SS. Finally, the repair template was chemically modified (phosphorothioate linkages) at the first and last two nucleotides to protect against nuclease degradation.

Genome editing of the TOP2 $\alpha$  E19/I19 5' SS was conducted as follows. Briefly, gRNA-2 (0.5  $\mu\text{g}$ ) was incubated with 2  $\mu\text{g}$  TrueCut Cas9 Protein v2 and 5  $\mu\text{M}$  TOP2 $\alpha$  E19/I19 repair template (designated

Enhanced E19/I19 5' SS/No PAM-2; Fig. 5E and Supplemental Table 1) for 15 minutes according to the manufacturer's instructions. This mixture was then transfected into K/VP.5 cells ( $2.25 \times 10^6$  cells in 100  $\mu$ l) by electroporation as reported previously (Kanagasabai et al., 2017). Forty-eight hours later, K/VP.5 cells (50,000) were lysed for Cas9 targeting and repair efficiency using the GCD assay described above. After verification of successful on-target genome editing generated by NHEJ, the remaining transfected K/VP.5 cells were plated using limiting dilution cloning in ten 96-well plates (0.8 cells per well). Aliquots (~25–50,000 cells) from single-cell clones were subsequently lysed with GCD buffer (see above) ~2 weeks after plating. Supernatants were assayed for HDR by genomic quantitative PCR (qPCR) using a probe specific for the edited TOP2 $\alpha$  E19/I19 5' SS (5'-TCATGCTGAGGTAAGTACACAATCC-3') to identify colonies with at least one TOP2 $\alpha$  edited allele. After the first round of transfection, multiple colonies with one edited allele were identified by qPCR and confirmed by sequencing. A single TOP2 $\alpha$  allele edited clone, designated K/VP.5/edit-1, was subjected to an additional round of transfection with gRNA-2, Cas9, and the TOP2 $\alpha$  E19/I19 repair template, followed by limiting dilution cloning. Genomic qPCR using a probe specific for the edited TOP2 $\alpha$  E19/I19 5' SS and the sub-optimal wild-type TOP2 $\alpha$  E19/I19 5' SS qPCR probe was used to identify gene-edited K/VP.5 clones with two and three TOP2 $\alpha$  edited alleles, now designated K/VP.5/edit-2 and K/VP.5/edit-3 (see Fig. 6).

**RsaI Restriction Enzyme Analysis of CRISPR/Cas9-Edited K/VP.5 Cells.** K/VP.5, K/VP.5/edit-1, K/VP.5/edit-2, and K/VP.5/edit-3 cells were lysed using cell GCD lysis buffer/Proteinase K as described above, and genomic DNA (1  $\mu$ l of lysate) at the TOP2 $\alpha$  locus between E18/intron 18/E19/I19 was PCR amplified (50  $\mu$ l reaction volume) using the following primers; GCD TOP2 $\alpha$  E18 forward (5'-GATCTATCCCTTCTATGGTGG-3') and GCD TOP2 $\alpha$  I19 reverse (5'-CA GAAATCAAAGGCAAGCAG-3'). Ten microliters of the PCR reaction was then digested by RsaI (cat. no. R0167S; New England Biolabs) according to the manufacturer's instructions. The digested and nondigested PCR products were fractionated by electrophoresis on a 2% agarose gel, and images were captured as described above (see Fig. 7).

**RNA Sequencing and Bioinformatics Analyses.** DNA-free RNA was isolated from K562, K/VP.5, and K/VP.5/edit-3 cells using the RNA Easy Plus Mini Kit (cat. no. 74134; Qiagen, Germantown, MD) with on-column digestion with RNase-Free DNase (cat. no. 79254). Two rounds of purification were used to assure high purity and DNase-free RNA isolation. RNA sequencing (RNA-seq) libraries were prepared at The Ohio State University Comprehensive Cancer Center Genomics Shared Resource and sequenced from quadruplicate samples from each cell line. Paired-end RNA-seq was performed on an Illumina HiSeq 4000 platform at the Genomics Services Laboratory of The Research Institute at Nationwide Children's Hospital, Columbus, OH. Illumina 150-bp paired-end RNA-seq raw reads from K562 and K/VP.5 RNA samples were mapped to the human reference genome GRCh38 using Hierarchical Indexing for Spliced Alignment for Transcripts version 2.1.0.9 (Kim et al., 2015), converted to bigwig coverage tracks using deepTools (Ramírez et al., 2016), and visualized using the Integrative Genomics Viewer (Robinson et al., 2011). Gene counts were generated with featureCounts (Liao et al., 2014) as described in Gadepalli et al. (2019). Gene expression was quantified as log<sub>2</sub> counts per million, and differential expression analysis was performed using R limma voom function (Ritchie et al., 2015). RNA-seq data are available in the Gene Expression Omnibus with accession number GSE163013.

**Growth Inhibitory Assays.** Log-phase K562 cells, K/VP.5 cells, and gene-edited K/VP.5 clonal cells were adjusted to  $1\text{--}1.5 \times 10^5$  cells per milliliter and incubated for 48 hours with DMSO as control solvent (final concentration 0.5%) and with various concentrations of a number of drugs, after which cells were counted on a model Z1 DUAL Coulter counter (Beckman Coulter, Indianapolis, IN). The extent of growth beyond the starting concentration in drug-treated versus control cells was expressed ultimately as percent inhibition of control growth. The

50% growth inhibitory values for each drug and each cell line were derived from replicate experiments performed on separate days fitting the concentration-response (inhibition) curves to a four-parameter logistic equation using Sigmaplot 14 (Systat Software, Inc., San Jose, CA).

**DNA Damage (Comet) Assays.** Alkaline (pH 13, detects primarily single-stranded breaks) single-cell gel electrophoresis (Comet) assays were performed according to the manufacturer's protocol (CometAssay Kit, cat. no. 4250-050-K; Trevigen, Gaithersburg, MD) and as previously described by our laboratory (Vlasova et al., 2011; Kanagasabai et al., 2017, 2018). Briefly, K562, K/VP.5, and K/VP.5/edit-3 cells were washed and resuspended in buffer (25 mM HEPES, 10 mM glucose, 1 mM MgCl<sub>2</sub>, 5 mM KCl, 130 mM NaCl, 5 mM NaH<sub>2</sub>PO<sub>4</sub>, pH 7.4). Cells were subsequently incubated with 2 or 10  $\mu$ M etoposide or DMSO (solvent control) for 30 minutes at 37°C. The treated cells were washed with ice-cold buffer and resuspended to  $0.28 \times 10^6$  cells per milliliter and then further diluted in low melt agarose. After alkaline electrophoresis (of ~2000 cells) and subsequent staining with a fluorescent DNA intercalating dye, SYBR Gold, the migrating fragments (comet tail) from the nucleoid (comet head) were visualized and the images captured by fluorescence microscopy. The Olive tail moment (Olive, 2002) was quantified by the ImageJ processing program with the open-source software tool OpenComet (Gyori et al., 2014; www.cometbio.org). Olive tail moments from more than 100 cells per sample condition were determined.

**Data Analysis.** Statistical analysis was performed using SigmaPlot 14. All data were expressed as means  $\pm$  S.D. Unless noted otherwise, groupwise differences were analyzed using a two-tailed paired Student's *t* test with no adjustment for multiple comparisons. A *P* value of less than 0.05 was considered statistically significant with 95% confidence intervals (CIs) noted in figure legends.

## Results

### TOP2 $\alpha$ Expression in Etoposide-Resistant K562 Cells.

Our laboratory previously established an etoposide-resistant K562 cell line by intermittent/continuous treatment with 0.5  $\mu$ M etoposide followed by limiting dilution to isolate and then characterize a clonal K/VP.5 cell line (Ritke and Yalowich, 1993; Ritke et al., 1994). Recent studies utilizing K/VP.5 cells established that TOP2 $\alpha$ /170 mRNA/protein levels were attenuated and TOP2 $\alpha$ /90 mRNA/protein levels were augmented compared with parental K562 cells (Kanagasabai et al., 2017, 2018; Elton et al., 2020). To recapitulate these findings, K562 and K/VP.5 cDNAs were subjected to qPCR utilizing TaqMan hydrolysis primers/probes. The results of these experiments demonstrated that TOP2 $\alpha$ /170 mRNA expression in K/VP.5 cells was reduced to 33% of that found in parental K562 cells, whereas TOP2 $\alpha$ /90 mRNA expression was increased 97-fold in K/VP.5 cells compared with parental K562 cells (Fig. 1A). In K562 cells, TOP2 $\alpha$ /90 mRNA levels were extremely low compared with TOP2 $\alpha$ /170 mRNA levels (Fig. 1A, light gray bars), whereas in K/VP.5 cells TOP2 $\alpha$ /90 mRNA levels exceeded those of TOP2 $\alpha$ /170 by ~2-fold (Fig. 1A, dark gray bars), reflecting I19 retention. Figure 1B also recapitulates our previous reports of decreased TOP2 $\alpha$ /170 protein in K/VP.5 cells, currently to a level 8% that of parental K562 cells, whereas TOP2 $\alpha$ /90 protein expression was 2-fold higher in K/VP.5 cells compared with K562 cells.

Since TOP2 $\alpha$ /90 heterodimerizes with TOP2 $\alpha$ /170 and is dominant-negative for etoposide-induced DNA damage and cytotoxicity compared with TOP2 $\alpha$ /170 homodimers (Kanagasabai et al., 2018), it was of interest that the ratio of TOP2 $\alpha$ /90 to

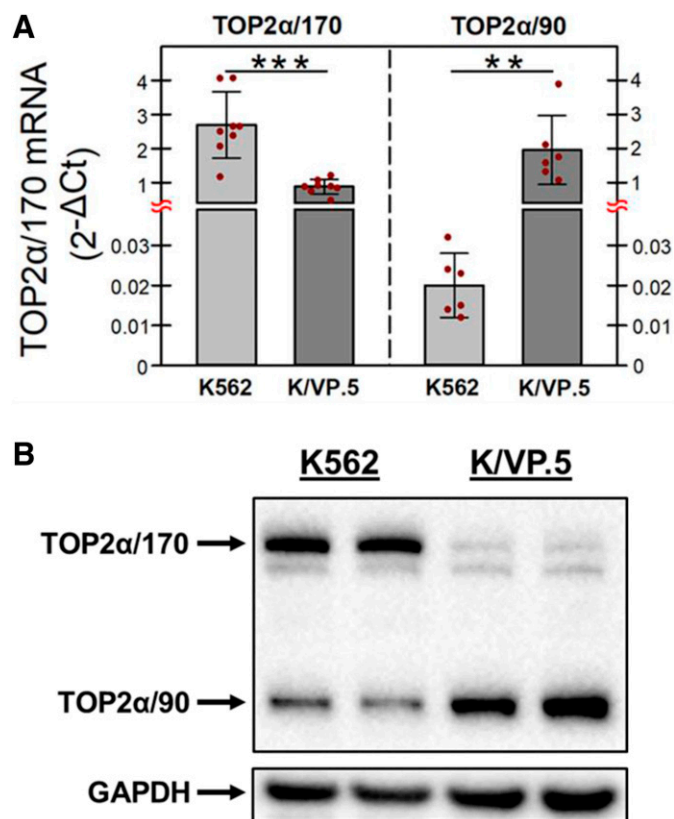


**Fig. 1.** TOP2 $\alpha$ /170 and TOP2 $\alpha$ /90 mRNA and protein levels in K562 and drug-resistant K/VP.5 cells. (A) qPCR experiments were performed utilizing K562 and K/VP.5 cDNAs and a TaqMan hydrolysis assay specific for TOP2 $\alpha$ /170 and TOP2 $\alpha$ /90 mRNAs. Results shown are means  $\pm$  S.D. from six or eight paired RNA/cDNA isolations/determinations performed on separate days;  $P < 0.001$ , comparing the differences in mean calculated  $2^{-\Delta C_t}$  values for K/VP.5 vs. K562 TOP2 $\alpha$ /170 mRNA, 95% CI (1.17, 2.46);  $P = 0.005$ , comparing the differences in mean calculated  $2^{-\Delta C_t}$  values for K/VP.5 vs. K562 TOP2 $\alpha$ /90 mRNA, 95% CI (0.87, 2.99). (B) Representative immunoblot analysis using K562 and K/VP.5 cellular lysates. Blots were probed with antibodies specific for the N-terminal portion of TOP2 $\alpha$ /170/90 (i.e., amino acids 14–27) or for GAPDH. \*\* $P < 0.01$ ; \*\*\* $P < 0.001$ .

TOP2 $\alpha$ /170 mRNA/protein was greater in resistant K/VP.5 compared with parental K562 cells (Fig. 1, A and B). Therefore, we next investigated whether there would similarly be an increase in the TOP2 $\alpha$ /90:TOP2 $\alpha$ /170 mRNA ratio in AML blasts from patients who relapsed after initial standard-of-care treatment with TOP2 $\alpha$ -targeted agents. Figure 2 demonstrated that, in six of seven patients, there was an increase in the TOP2 $\alpha$ /90:TOP2 $\alpha$ /170 mRNA ratios pretreatment and after relapse. Evaluation of the mean values for TOP2 $\alpha$ /90:TOP2 $\alpha$ /170 mRNA ratios pretreatment and after relapse for all seven patients indicated an average 4.01-fold increase that was statistically significant [ $P = 0.036$ ; 95% CI (1.14, 14.16)]. These results suggested that the TOP2 $\alpha$ /90 to TOP2 $\alpha$ /170 ratio may be a correlate/determinant of acquired drug resistance and pointed to the potential importance of alternative RNA processing/intron retention as a biomarker and/or as a target for modulation/circumvention of drug resistance to TOP2 $\alpha$ -targeted agents.

**TOP2 $\alpha$  Minigene Constructs for Evaluation of I19 Retention.** Our laboratory previously demonstrated that the TOP2 $\alpha$ /90 isoform is the translation product of an mRNA that shares the first 19 exons with the TOP2 $\alpha$ /170 transcript (Kanagasabai et al., 2017). However, the TOP2 $\alpha$ /90 mRNA

retains a processed I19 and lacks the published TOP2 $\alpha$ /170 transcript sequences from exon 20 to exon 35 (Kanagasabai et al., 2017, 2018; Elton et al., 2020). As a result of I19 retention, TOP2 $\alpha$ /90 (i.e., 786 amino acids, 90,076 Da) is approximately one-half the size of the wild-type TOP2 $\alpha$ /170 protein (i.e., 1531 amino acids, 174,385 Da) and does not harbor the active site tyrosine (Tyr-805) required for wild-type TOP2 $\alpha$ /170 to generate DNA strand breaks (Deweese and Osheroff, 2009; Nitiss, 2009), which may account for its dominant-negative effects upon heterodimerization with TOP2 $\alpha$ /170 (Kanagasabai et al., 2018).

To examine the mechanism(s) responsible for TOP2 $\alpha$  I19 retention and resultant increased TOP2 $\alpha$ /90 protein levels, our laboratory generated a minigene expression construct (Cooper, 2005), designated TOP2 $\alpha$ /Minigene1, which incorporated E19, I19, and E20 (Fig. 3A). To measure the relative expression levels of surrogate TOP2 $\alpha$ /170 mRNAs (E19/E20; i.e., I19 spliced out) transcribed and processed from the plasmid, TOP2 $\alpha$ /Minigene1 was transiently transfected into K562 and K/VP.5 cells, and total RNA was isolated, treated with DNase I, and then reverse-transcribed for PCR. To ensure that only minigene-expressed mRNAs were amplified, a T7 primer (forward) was used in all PCR reactions (Fig. 3A). PCR analysis of the minigene-expressed TOP2 $\alpha$ /170 mRNAs demonstrated that I19 was appropriately spliced out (224-bp amplicon) in both K562 and K/VP.5 cells and that K562 cells exhibited higher levels of properly processed TOP2 $\alpha$ /170 mRNAs (Fig. 3B). Importantly, the minigene analysis correlated with the qPCR data shown in Fig. 1A, which demonstrated that TOP2 $\alpha$ /170 mRNA expression levels were greater in K562 compared with K/VP.5 cells. Therefore, transfection of the TOP2 $\alpha$  gene fragment (i.e., E19, I19, and E20) within TOP2 $\alpha$ /Minigene1 recapitulated the TOP2 $\alpha$ /170 mRNA expression levels observed in nontransfected K562 and K/VP.5 cells (Fig. 1A) indicating that RNA processing of the TOP2 $\alpha$ /Minigene1-derived transcripts mimics endogenous TOP2 $\alpha$  mRNA splicing at the E19/I19 boundary and is amenable for further mechanistic studies.

Enhanced TOP2 $\alpha$  I19 retention observed in K/VP.5 compared with K562 cells is likely the result of a combinatorial effect of *cis*-element SS sequences and the dysregulation of *trans*-acting factors (Lee and Rio, 2015; Monteuis et al., 2019). *Cis*-elements are recognition sequences used by splicing-initiating factors to recruit the splicing machinery, and the recognition efficiency of SS is governed by base pair homology with these splicing-initiating factors (Lee and Rio, 2015; Monteuis et al., 2019). Interestingly, the TOP2 $\alpha$  E19/I19 5' SS is suboptimal (GAG//GTAAAC), differing from the consensus splice site (CAG//GTAAGT) by three nucleotides, and has a splicing "score" of 6.1 out of a maximum of 12.4 (Splice Site Score Calculation).

To investigate whether the weak TOP2 $\alpha$  E19/I19 5' SS contributes to I19 retention, the wild-type 5' SS was mutated from GAG//GTAAAC to CAG//GTAAGT to generate the consensus TOP2 $\alpha$  E19/I19 5' SS in the TOP2 $\alpha$ /Minigene1 construct (designated TOP2 $\alpha$ /Minigene2) (Fig. 3C). K/VP.5 cells were transiently transfected with the suboptimal wild-type 5' SS minigene (TOP2 $\alpha$ /Minigene1) or with the consensus 5' SS minigene (TOP2 $\alpha$ /Minigene2) construct. The relative expression of the surrogate TOP2 $\alpha$ /90 and TOP2 $\alpha$ /170 mRNAs transcribed and processed from the minigenes was determined by multiplex PCR using a T7 forward primer and TOP2 $\alpha$ /90

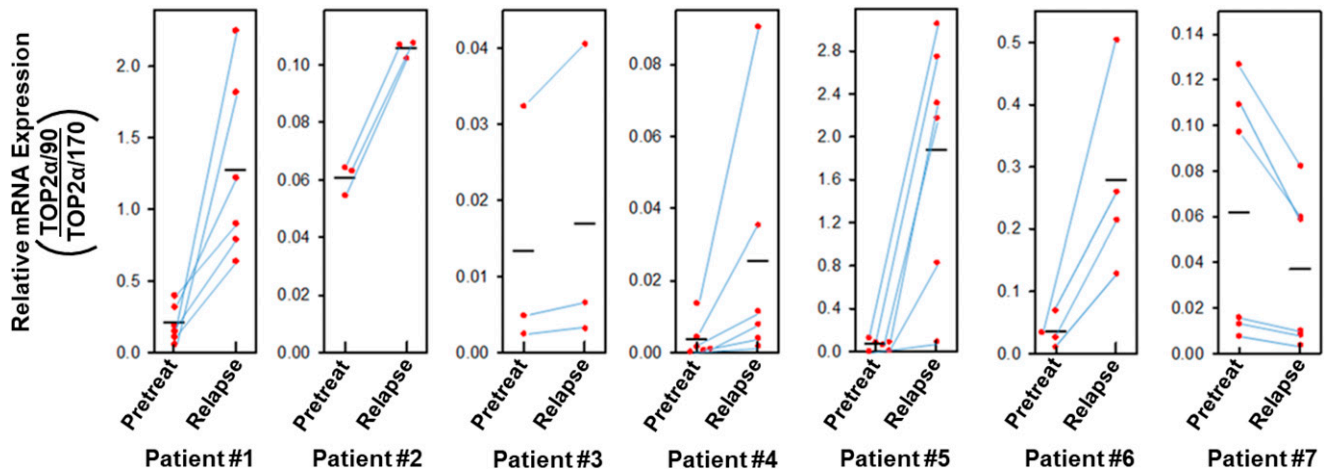


**Fig. 2.** Effects on TOP2 $\alpha$ /90:TOP2 $\alpha$ /170 mRNA ratios in patients with AML upon post-therapy relapse. Total RNA samples were isolated from blast cells obtained from patients newly diagnosed with AML and the same patients at relapse, after receiving TOP2 $\alpha$ -targeting therapy. qPCR experiments were performed utilizing TaqMan hydrolysis probes specific for TOP2 $\alpha$ /170 and TOP2 $\alpha$ /90 mRNAs as described in *Materials and Methods* and as used previously (Kanagasabai et al., 2017). From each patient's samples (pretreatment and at relapse), cDNAs were generated in parallel from isolated RNAs by reverse transcription, and qPCR reactions were subsequently performed in parallel using a common master reaction mix. In addition, these evaluations were repeated on separate days by generation of cDNAs with subsequent qPCR reactions performed from each pair of patient's samples. The ratio of TOP2 $\alpha$ /90:TOP2 $\alpha$ /170 mRNA pretreatment and after relapse was calculated and plotted as coordinate plots with point-line-point connections for each pair of evaluations for each patient. For patient #1, one of the sets of values connected by point-line-point for pretreatment (0.4) and relapse (0.9) were indicated in a previous publication (Kanagasabai et al., 2018). The black horizontal bars represent the mean values from repeated paired measures. Evaluation of the mean values for TOP2 $\alpha$ /90:TOP2 $\alpha$ /170 mRNA ratios pretreatment and after relapse for all seven patients indicated an average 4.01-fold increase that was statistically significant after performing a paired *t* test on log transformed values;  $P = 0.036$  [95% CI (1.14, 14.16)].

and TOP2 $\alpha$ /170 specific reverse primers (Fig. 3A; *Materials and Methods* and Supplemental Table 1).

Multiplex PCR analysis of the minigene-expressed mRNAs in K/VP.5 cells transfected with the wild-type 5' SS TOP2 $\alpha$ /Minigene1 construct demonstrated that the TOP2 $\alpha$ /90 mRNA (E19/I19; i.e., I19 retained) 350-bp amplicon levels were greater than the TOP2 $\alpha$ /170 mRNA (E19/E20, I19 spliced out) 224-bp amplicon levels at PCR cycles 33 and 35 (Fig. 3C). In contrast, multiplex PCR analysis of the minigene-expressed mRNAs in K/VP.5 cells transfected with the consensus 5' SS TOP2 $\alpha$ /Minigene2 construct demonstrated that TOP2 $\alpha$ /170 mRNA (E19/E20, I19 spliced out) 224-bp amplicon levels were now greater than the TOP2 $\alpha$ /90 (E19/I19; I19 retained) 350-bp amplicon levels (Fig. 3C). Hence, optimizing the TOP2 $\alpha$  E19/I19 5' SS resulted in reduced intron retention, decreased surrogate TOP2 $\alpha$ /90 mRNA expression, and increased surrogate TOP2 $\alpha$ /170 mRNA (Fig. 3C). These promising preliminary results prompted our use of CRISPR/Cas9 gene editing to optimize the TOP2 $\alpha$  E19/I19 5' SS, diminish I19 retention in K/VP.5 cells, increase TOP2 $\alpha$ /170 expression, and circumvent drug resistance.

**gRNA-2 Directs Cas9 Cleavage in the TOP2 $\alpha$  E19/I19 Boundary Sequence.** Our results above with the TOP2 $\alpha$  minigene plasmids, together with previously published findings (Wickramasinghe et al., 2015; Yue and Ogawa, 2018), clearly demonstrated that optimizing a weak 5' SS can improve the efficiency of intron removal. Therefore, we next used the CRISPR/Cas9 system (Jinek et al., 2012; Mali et al., 2013; Liang et al., 2017) to introduce specific gene edits in the suboptimal TOP2 $\alpha$  E19/I19 5' SS through HDR to enhance splicing out of I19. The gRNA/Cas9 complex binds to the target site, and the Cas9 nuclease introduces a blunt-end DSB three bases upstream of a three-nucleotide sequence motif (NGG), known as the protospacer-adjacent motif (PAM) (Jinek et al., 2012; Mali et al., 2013). Thus, the

TOP2 $\alpha$  E19/I19 boundary sequence (200 bp) was analyzed for PAM sequence motifs utilizing the CRISPR/Cas9 Target Online Predictor (CCTop) (<https://cctop.cos.uni-heidelberg.de/>) (Stemmer et al., 2015). Although 12 PAM sites were identified (not shown), only three candidate PAM/gRNAs (Fig. 4A, color-coded) were examined since they would target Cas9 in close proximity to the intended mutations (Fig. 5), which should maximize editing efficiency (Paquet et al., 2016; Liang et al., 2017). Of the three PAM/gRNAs studied, PAM/gRNA-2 had the highest CRISPRater efficacy score of 0.71 compared with 0.60 for PAM/gRNA-1 and 0.50 for PAM/gRNA-3 (Labuhn et al., 2018).

To determine the most efficient PAM/gRNA site, each corresponding gRNA was complexed with Cas9 and transiently transfected into K/VP.5 cells. Forty-eight hours post-transfection, cells were assayed for indels created by NHEJ (Qi et al., 2013) due to Cas9 cleavage in the TOP2 $\alpha$  E19/I19 boundary sequence. Briefly, cells were lysed using the GCD lysis buffer, followed by PCR using a forward primer on E18 and a reverse primer on I19 to amplify the CRISPR/Cas9 target region (Fig. 4B). PCR amplicons were then denatured and reannealed to evaluate Cas9-induced breaks and NHEJ-mediated mismatches (heteroduplex DNA) targeted/cleaved by T7 endonuclease I. GCD analysis of PAM/gRNAs 1–3 revealed that only PAM-2/gRNA-2 (color-coded red) effectively guided Cas9 to the target site (Fig. 4C). The calculated Cas9 cleavage efficiency (Liang et al., 2017) in the TOP2 $\alpha$  E19/I19 boundary by the TOP2 $\alpha$  gRNA-2 was 7.3% compared with the optimized control HPRT1 gRNA of 14.0%. All subsequent experiments were performed with TOP2 $\alpha$  gRNA-2.

**CRISPR/Cas9: Strategy to Edit the TOP2 $\alpha$  E19/I19 5' SS.** Since the wild-type TOP2 $\alpha$  E19/I19 5' SS is suboptimal (GAG/GTAAAC) (Fig. 5A, blue box), analyses were performed to determine the impact of specific gene edits on the 5' SS scores. These analyses demonstrated that if the TOP2 $\alpha$  E19/I19 5' SS

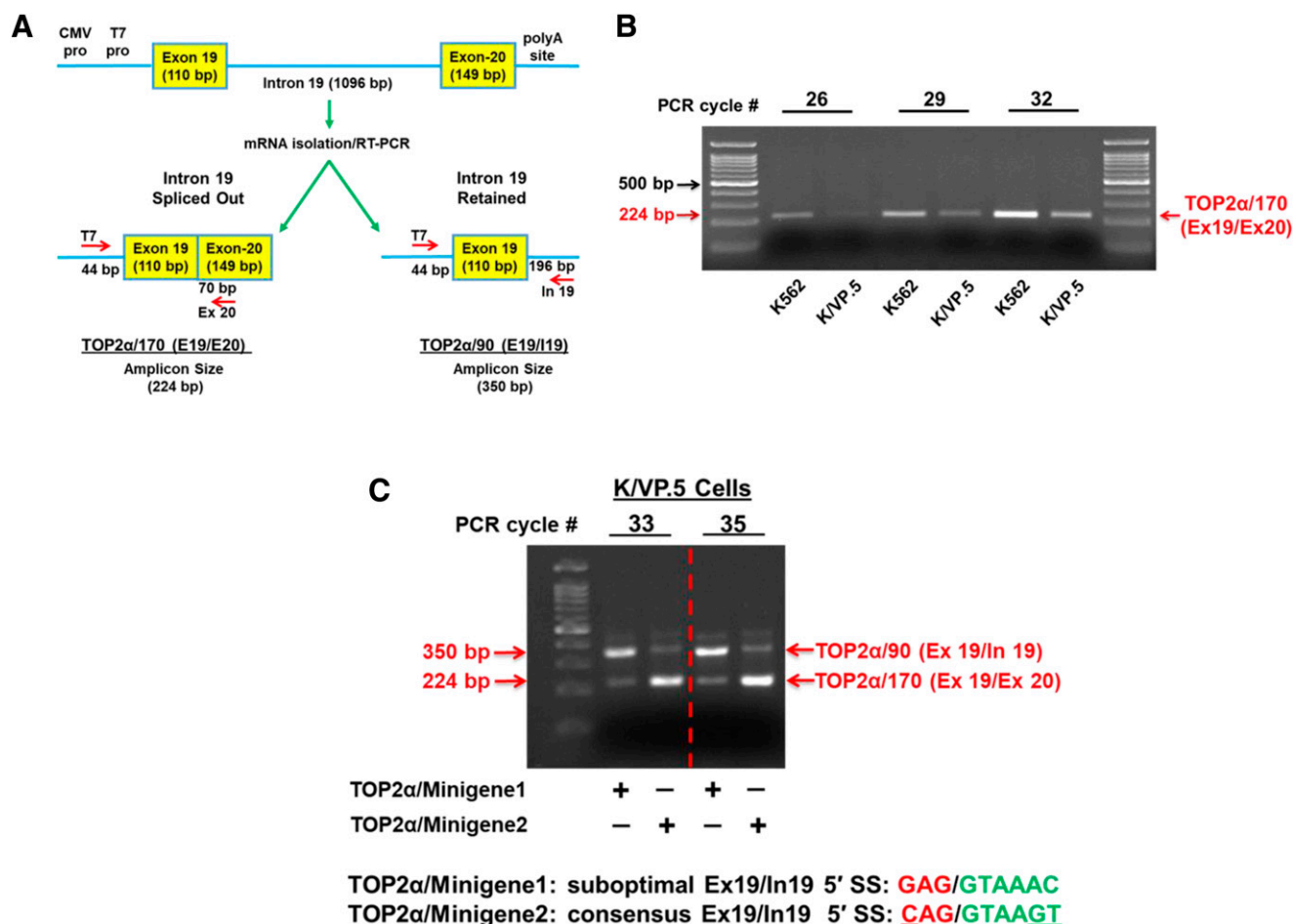


**Fig. 3.** Effects of optimizing the weak TOP2 $\alpha$  E19/I19 5' SS harbored in a TOP2 $\alpha$  minigene construct on TOP2 $\alpha$ /170 mRNA expression in etoposide-resistant K/VP.5 cells. (A) Schematic representation of the TOP2 $\alpha$  gene segment that was subcloned into the pcDNA3.1 expression plasmid. Minigene-expressed and processed TOP2 $\alpha$ /170 (E19/E20; i.e., I19 spliced out) and TOP2 $\alpha$ /90 (E19/I19; i.e., I19 retained) PCR amplicon sizes are shown. CMV, cytomegalovirus; polyA, XXXX; pro, promoter. (B) K562 and K/VP.5 cells were transfected with the TOP2 $\alpha$ /Minigene1 construct (i.e., harboring the weak TOP2 $\alpha$  E19/I19 5' SS). RNA was isolated and reverse transcribed, and PCR experiments were performed. Ethidium bromide-stained agarose gel fractionated TOP2 $\alpha$ /170 amplicons are denoted with the red arrow. The PCR cycle number is indicated to ensure the linear range of amplification and allows for the direct comparison of the intensity of the TOP2 $\alpha$ /170 amplicon from K562 cells versus K/VP.5 cells. (C) K/VP.5 cells were cotransfected with TOP2 $\alpha$ /Minigene1 and TOP2 $\alpha$ /Minigene2 (i.e., harboring a consensus TOP2 $\alpha$  E19/I19 5' SS). RNA was isolated and reverse transcribed, and multiplex PCR experiments were performed. Ethidium bromide-stained agarose gel fractionated TOP2 $\alpha$ /90 and TOP2 $\alpha$ /170 amplicons are denoted. The PCR cycle number is indicated to ensure the linear range of amplification and allows for the direct comparison of the intensity of the TOP2 $\alpha$ /90 and TOP2 $\alpha$ /170 amplicon from K/VP.5 cells.

(splicing “score” of 6.1) was edited to a consensus 5' SS (splicing “score” of 12.4) (Splice Site Score Calculation), as was done for the TOP2 $\alpha$ /Minigene2 construct (Fig. 3C), then a nonconservative amino acid change would result (Glu→Gln) in the TOP2 $\alpha$ /170 protein (Fig. 5B, blue box). In contrast, by editing only the last two nucleotides of the TOP2 $\alpha$  E19/I19 5' SS (AC→GT) (Fig. 5C), the 5' SS score would be enhanced (from 6.1→11.6) with no amino acid change in the TOP2 $\alpha$ /170 protein sequence (compare Fig. 5, A and C). Therefore, we initially planned to include only the AC→GT nucleotide change (Fig. 5C) in the mutagenic single-stranded oligo DNA nucleotide (ssODN) repair template (not shown). However, K562 and drug-resistant K/VP.5 cells are triploid with three copies of the TOP2 $\alpha$  gene (Cioe et al., 1981; Zhou et al., 2019), presenting challenges for successful isolation of a clone with gene editing of the E19/I19 5' SS in all three alleles after a single Cas9, gRNA, repair template cotransfection.

Since only PAM-2/gRNA-2 effectively guided Cas9 to the target site (Fig. 4C), a repair template was designed based on the TOP2 $\alpha$  E19/I19 gene boundary sequences changes shown

in Fig. 5D to include the AC→GT alterations and to eliminate PAM-2. This strategy was implemented to avoid recutting of already edited alleles upon subsequent rounds of transfection, to assure editing of all three TOP2 $\alpha$  alleles, and to result in an optimized TOP2 $\alpha$  E19/I19 5' SS. The G→C modification in the PAM-2 site (Fig. 5, D and E) resulted in a very conservative amino acid change, Gly→Ala (compare Fig. 5, A and D), in the TOP2 $\alpha$  protein. The symmetric 180-nucleotide ssODN HDR template (Fig. 5E, denoted as Enhanced E19/I19 5' SS/No PAM-2) with homology to both TOP2 $\alpha$  E19 and I19 was synthesized and used in all CRISPR/Cas9 transfection experiments.

**CRISPR/Cas9: qPCR Selection and Sequence Analysis of Edited TOP2 $\alpha$  E19/I19 Clonal Cell Lines.** K/VP.5 cells were transfected with gRNA-2 (Fig. 4A; Supplemental Table 1), Cas9 protein, and the HDR template (Fig. 5E). Forty-eight hours post-transfection, cells were seeded at 0.8 cells per well in 96-well plates and allowed to grow for 2 weeks. Cell aliquots harvested from single-colony wells were lysed and screened by genomic DNA qPCR.

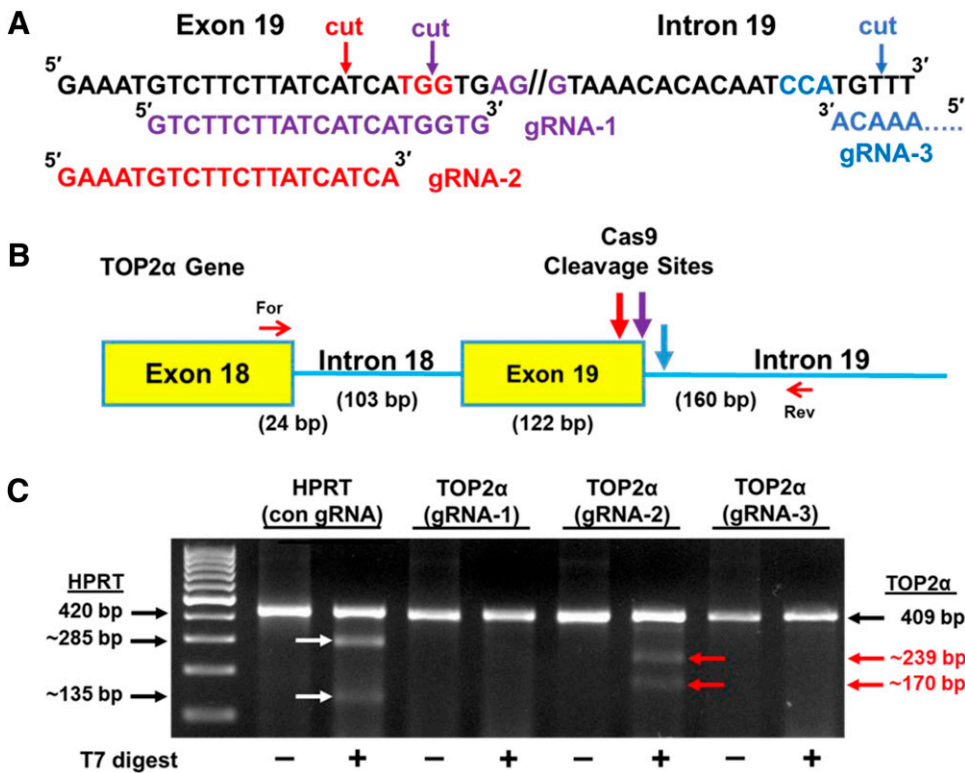


**Fig. 4.** Effects of gRNA-2 on Cas9 cleavage at the TOP2 $\alpha$  E19/I19 5' boundary sequence. (A) Sequence of the TOP2 $\alpha$  E19/I19 5' boundary sequence is shown. Candidate PAM sites and corresponding gRNAs are color coded. Arrows denote where Cas9 will generate a DSB. (B) Schematic representation of the E18 through I19 region of the TOP2 $\alpha$  gene. The large color-coded arrows denote sites where gRNA-directed Cas9 cleavage and NHEJ generation of indels can occur. The small red arrows denote the forward (For) and reverse (Rev) primers used for the GCD assay. (C) Ethidium bromide-stained agarose gel fractionated GCD PCR amplicons before and after treatment with T7 endonuclease I. The parental and T7 endonuclease I cleaved daughter PCR amplicons are indicated, and their respective sizes are denoted. A positive HPRT1 control (con) GCD assay is also shown.

We have previously validated the specificity of a qPCR hybridization probe (5'-TCATGGTGAGGTAAACACACAATCC-3') for the wild-type TOP2 $\alpha$  E19/I19 boundary to demonstrate that the TOP2 $\alpha$ /90 truncated isoform was encoded by an mRNA that harbors a retained and processed I19 (Kanagasabai et al., 2017, 2018; Elton et al., 2020). To discriminate between the wild-type TOP2 $\alpha$  E19/I19 and the CRISPR/Cas9-edited TOP2 $\alpha$  E19/I19 boundary, an additional custom qPCR hybridization probe containing the edited sequence (5'-TCATGCTGAGGTAAGTACACAATCC-3') was synthesized. Nontransfected K/VP.5 cell control experiments demonstrated no signal from this custom E19/I19 edited qPCR probe (Fig. 6AI, red line). Only the wild-type TOP2 $\alpha$  E19/I19 boundary probe (black line) yielded a positive genomic qPCR signal (Fig. 6AI). Sanger sequencing verified the wild-type TOP2 $\alpha$  genomic sequence (Fig. 6BI). In contrast, when CRISPR/Cas9-edited K/VP.5 cell lysates were screened (~60 clonal cell colonies), several clones were identified where the qPCR signal for the edited TOP2 $\alpha$  E19/I19 boundary probe signal (red line) appeared a few PCR cycles after the wild-type (black line) TOP2 $\alpha$  E19/I19 boundary probe (Fig. 6AII). Sanger sequence analysis demonstrated that both wild-type and edited genomic sequence were present in the TOP2 $\alpha$  E19/I19 boundary, with the wild-type sequence predominant at all three of the edited sites (Fig. 6BII). Together, these results suggested that one of the three TOP2 $\alpha$  E19/I19 boundary alleles was edited in this clonal cell line (now designated K/VP.5/edit-1).

The K/VP.5/edit-1 clonal cell line was subjected to an additional transfection with gRNA-2, Cas9 protein, and the TOP2 $\alpha$  HDR template. Forty-eight hours post-transfection, K/VP.5/edit-1 cells were seeded at 0.8 cells per well, grown 2 weeks followed by screening of cell lysates from single clonal colonies by genomic DNA qPCR utilizing the wild-type

and CRISPR/Cas9-edited TOP2 $\alpha$  E19/I19 boundary probes. From the second transfection (~60 clonal colonies screened), a clonal cell population was identified where the edited TOP2 $\alpha$  E19/I19 boundary probe signal (red line) appeared earlier than the wild-type (black line) TOP2 $\alpha$  E19/I19 boundary probe (Fig. 6AIII). Sanger sequence analysis again demonstrated that both wild-type and edited genomic sequences were present in the TOP2 $\alpha$  E19/I19 boundary (Fig. 6BIII). However, the CRISPR/Cas9-edited sequence was now predominant in the electropherogram at all three mutated sites (Fig. 6BIII). Together, these results suggested that two of the three TOP2 $\alpha$  E19/I19 boundary alleles were edited in this clonal cell line (now designated K/VP.5/edit-2).

Finally, from this same second transfection, another clonal cell line was identified where the genomic qPCR results of a cellular lysate yielded a positive PCR signal (red line) only with the edited TOP2 $\alpha$  E19/I19 boundary probe (Fig. 6AIV), suggesting that all three TOP2 $\alpha$  E19/I19 boundary alleles were edited. Sanger sequence analysis verified that only the edited sequence was present all three mutated sites (Fig. 6BIV) in this clonal cell line (now designated K/VP.5/edit-3).

**RsaI Analysis Validation of CRISPR/Cas9 Editing of the TOP2 $\alpha$  E19/I19 5' SS in K/VP.5 Cells.** Fortuitously, editing the last two nucleotides of the TOP2 $\alpha$  E19/I19 5' SS (AC $\rightarrow$ GT) (Fig. 5C) introduced a restriction site for RsaI endonuclease (GT $\downarrow$ AC). Successful TOP2 $\alpha$  gene editing would allow for RsaI digestion at the E19/I19 boundary. Thus, an independent assay with RsaI endonuclease was carried out to validate the CRISPR-edited TOP2 $\alpha$  gene clones. Cell lysates from the CRISPR-generated cell lines (K/VP.5/edit-1 $\rightarrow$ K/VP.5/edit-3) and parental K/VP.5 cells were used as templates for PCR reactions performed with a forward primer that anneals to TOP2 $\alpha$  E18 and a reverse primer that anneals to I19





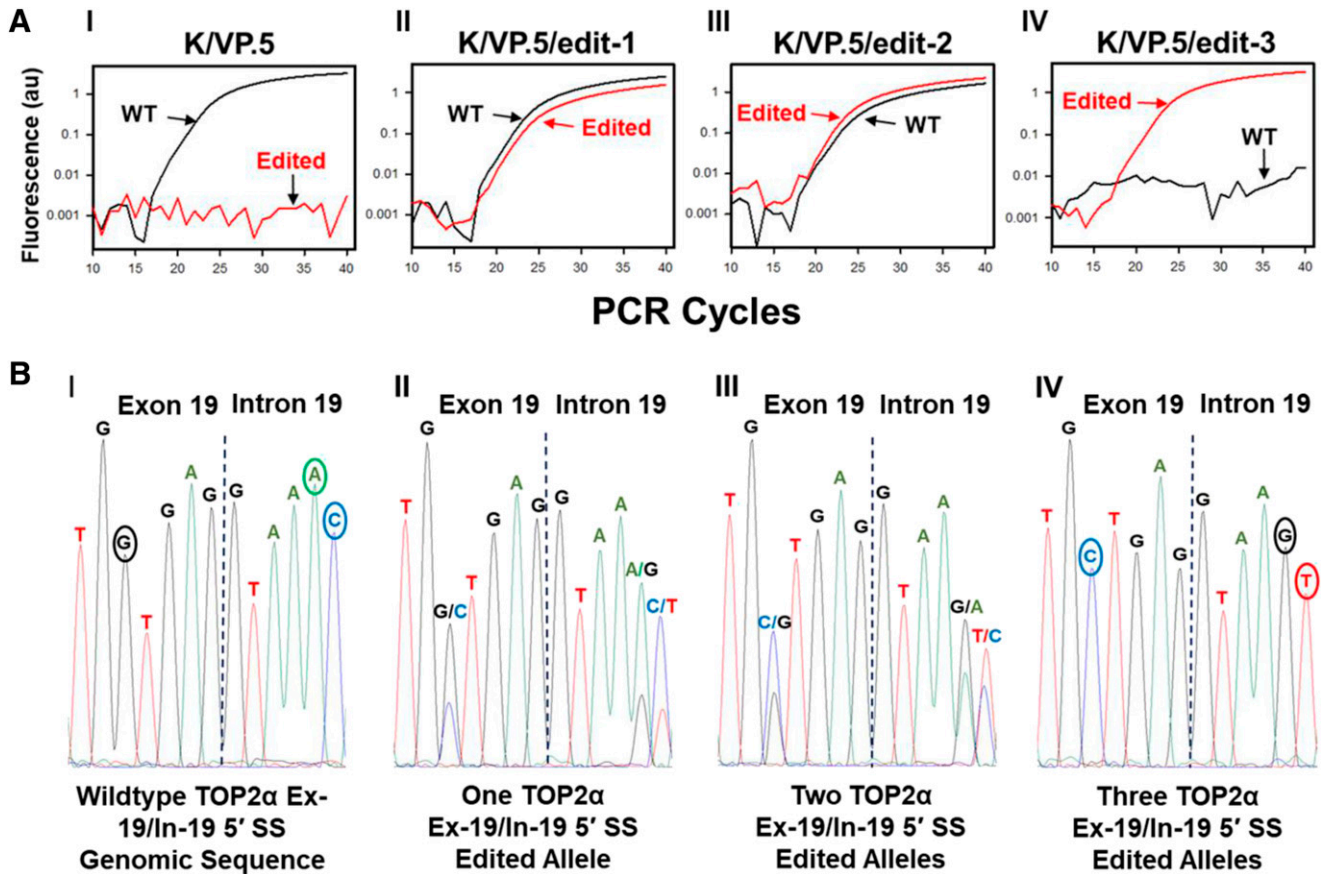


**Fig. 6.** qPCR selection and sequence analysis of CRISPR/Cas9-edited TOP2 $\alpha$  E19/I19 5' SS clonal cell lines. (A) Amplification plots of qPCR reactions from K/VP.5 and K/VP.5/edit-1,2,3 cells (labeled I–IV) using wild-type and edited, specific E19/I19 boundary qPCR probes. (B) Electropherograms of the genomic sequence of the TOP2 $\alpha$  E19/I19 gene boundary in K/VP.5 and K/VP.5/edit-1–3 cells (labeled I–IV).

(Fig. 8A, C and D), we next evaluated whether etoposide activity in this gene-edited clonal cell line would be enhanced consistent with circumvention of resistance.

Alkaline single-cell gel electrophoresis (Comet) assays (Olive, 2002) were performed to assess DNA strand breaks (Olive Tail Moment) in K562, K/VP.5, and K/VP.5/edit 3 cells incubated for 30 minutes with 2 and 10  $\mu$ M etoposide (Fig. 9A). Etoposide induced concentration-dependent DNA strand breaks in K562 cells, which were attenuated in resistant K/VP.5 cells and restored in K/VP.5/edit-3 cells to levels comparable to those in the parental K562 cells. As performed (at pH 13), Comet assays detected primarily single-stranded breaks (Luke et al., 2010). Therefore, etoposide-induced DNA DSBs were also evaluated using expression of phosphorylated H2AX ( $\gamma$ H2AX) as an endpoint (Rogakou et al., 1998). Cells were incubated for 30 minutes with DMSO solvent control or etoposide (10–50  $\mu$ M) followed by lysis and immunoblotting with anti- $\gamma$ H2AX antibody. Etoposide induced a concentration-dependent expression of  $\gamma$ H2AX in all three cell lines with evident attenuation of DSBs in resistant K/VP.5 cells and restoration of etoposide-induced DSBs in K/VP.5/edit-3 cells (Fig. 9B). These results were consistent with the profile observed with Comet assays assessing single-stranded breaks (Fig. 9A). Quantitation of  $\gamma$ H2AX results from five experiments performed on separate days demonstrated a concentration-dependent increase in etoposide-induced  $\gamma$ H2AX in all three cells

lines, with a statistically significant increase in DSBs induced in K562 cells ( $P = 0.023$ ) and K/VP.5/edit-3 cells ( $P < 0.001$ ) compared with K/VP.5 cells at 50  $\mu$ M etoposide (Fig. 9C).

In parallel with increased etoposide-induced DSBs ( $\gamma$ H2AX), there was concentration-dependent “band depletion” of TOP2 $\alpha$ /170 in K562, K/VP.5, and K/VP.5/edit-3 cells (Fig. 9B), consistent with etoposide-induced formation of high molecular weight TOP2 $\alpha$ /DNA covalent complexes prevented from entering gels (Kaufmann and Svingen, 1999). At 50  $\mu$ M etoposide there was a statistically significant depletion of TOP2 $\alpha$ /170 compared with DMSO controls in all three cell lines (Fig. 9D). In contrast, there was no statistically significant decrease in TOP2 $\alpha$ /90 consistent with the lack of active site Tyr-805 in this truncated isoform (Kanagasabai et al., 2017, 2018) and the presumed loss of ability to form covalent complexes with DNA. Together, drug-induced DNA damage studies (Fig. 9, A and B) support the hypothesis that optimizing the TOP2 $\alpha$  E19/I19 5' SS sensitizes previously resistant K/VP.5 cells as a consequence of 1) enhanced splicing out of I19, 2) reduced production of TOP2 $\alpha$ /90, and 3) restoration of TOP2 $\alpha$ /170 levels.

Next, 48-hour growth inhibition assays were performed in K562, K/VP.5, and K/VP.5/edit cells treated continuously with etoposide, other TOP2 $\alpha$ -targeted agents, the topoisomerase I inhibitor camptothecin, and the microtubule inhibitor podophyllotoxin (Fig. 10; Table 1). Compared with K562 cells, K/VP.5 cells were 21-fold resistant to etoposide, with complete circumvention of resistance observed in K/VP.5/edit-3

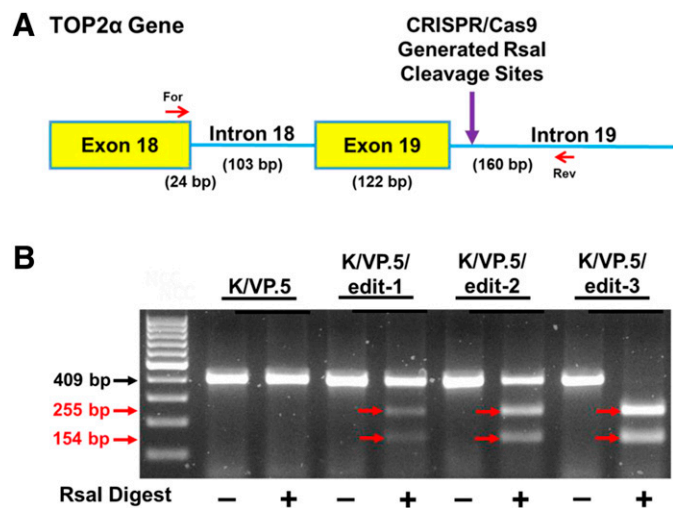


**Fig. 7.** Validation of CRISPR/Cas9 editing of the TOP2 $\alpha$  E19/I19 5' SS in K/VP.5 cells by RsaI analysis. (A) Schematic representation of the E18 through I19 portion of the TOP2 $\alpha$  gene. Red arrows denote the forward (For) and reverse (Rev) primers used for the identification of CRISPR editing of the TOP2 $\alpha$  E19/I19 5' SS using RsaI endonuclease. Purple arrow denotes site where RsaI creates double-stranded breaks of CRISPR-edited PCR amplicons (B) Ethidium bromide-stained agarose gel of fractionated RsaI-treated PCR amplicons from K/VP.5 and K/VP.5/edit-1–3 DNA. The black arrow denotes the parental PCR amplicon. Expected sizes of parental and daughter PCR amplicons are indicated in red.

cells (Fig. 10A; Table 1). Separate experiments in K562, K/VP.5, K/VP.5/edit-1, KVP.5/edit-2, and K/VP.5/edit-3 cells revealed a progressive restoration of TOP2 $\alpha$ /170 protein levels compared with K562 cells (Supplemental Fig. 1). Moreover, based on IC<sub>50</sub> values from replicate etoposide-induced growth inhibition assays (Supplemental Fig. 2; Supplemental Table 2), there was partial but progressive reversal of resistance in the one TOP2 $\alpha$  allele- and two TOP2 $\alpha$  allele-edited K/VP.5/edit-1 and K/VP.5/edit-2 cells, respectively, with complete circumvention of resistance in K/VP.5/edit-3 cells, consistent with results shown in Fig. 10 and Table 1. These results validate the import of the E19/I19 5' SS for intron retention, expression of TOP2 $\alpha$ /170 mRNA/protein, and drug sensitivity. Of note, doubling times for all five cell lines were similar (Supplemental Table 2), indicating that gene editing did not alter growth characteristics.

Figure 10 and Table 1 also indicated 5–30-fold crossresistance to teniposide, daunorubicin, mAMSA, pixantrone, and mitoxantrone, respectively (Table 1). As with etoposide, complete circumvention of resistance was observed with teniposide (Table 1) and daunorubicin (Fig. 10B; Table 1) in K/VP.5/edit-3 cells, whereas resistance was extensively but not completely reversed with mAMSA (Fig. 10C), mitoxantrone (Fig. 10D), and pixantrone (Fig. 10E; Table 1). Finally, there was no resistance to camptothecin (Fig. 10F; Table 1) or podophyllotoxin (Table 1) in K/VP.5 or K/VP.5/edit-3 cells compared with K562 cells, thus validating the specificity of the resistance phenotype in K/VP.5 cells for TOP2 $\alpha$ -targeted agents and indicating that gene editing did not impact the sensitivity to two agents with intracellular targets differing from TOP2 $\alpha$ . Together, the results were again consistent with optimization of the E19/I19 5' SS playing an important role in diminishing intron retention leading to restored TOP2 $\alpha$ /170 mRNA/protein and greater sensitivity to TOP2 $\alpha$ -targeting agents.

## Discussion

Chemoresistance to TOP2 $\alpha$ -targeted agents can result from a number of molecular mechanisms (Ganapathi and Ganapathi, 2013; Capelôa et al., 2020). In the case of K/VP.5 cells, acquired resistance to etoposide and similar TOP2 $\alpha$  poisons is due, in part, to decreased TOP2 $\alpha$ /170 expression associated with the increased expression of a C-terminal truncated isoform, TOP2 $\alpha$ /90 (Fig. 1, A and B), as a result of intron 19 retention and processing (Kanagasabai et al., 2017, 2018). Importantly, the truncated TOP2 $\alpha$ /90 isoform lacks the active site Tyr-805 required to generate DNA strand breaks and is a determinant of chemoresistance through a dominant-negative effect related to heterodimerization with TOP2 $\alpha$ /170, leading to reduced drug-induced TOP2 $\alpha$ /170-DNA covalent cleavage complexes, attenuated DNA damage, and decreased cytotoxic action (Kanagasabai et al., 2017, 2018).

Intron retention affects ~80% of protein coding genes in humans and is characterized by the inclusion of one or more introns in mature mRNA transcripts (Middleton et al., 2017). The SS sequences that define the 5' and/or 3' SS retained introns are often weak (Monteuuis et al., 2019). Importantly, several studies have demonstrated that the strengthening of a weak 5' SS by mutagenesis could enhance the splicing out of retained introns (Huang et al., 2012; Wickramasinghe et al., 2015; Eckert et al., 2016; Yue et al., 2017). Here, we used CRISPR/Cas9 gene editing to optimize the weak TOP2 $\alpha$  E19/I19 5' SS in K/VP.5 cells to improve splicing and circumvent drug resistance.

The CRISPR/Cas9 gene editing system requires a gRNA, which comprises the crRNA (required for DNA targeting) and the tracrRNA (necessary for nuclease activity) (Jinek et al., 2012; Cong et al., 2013; Mali et al., 2013). To direct the Cas9 nuclease, the 20-nucleotide crRNA sequence must be complementary to the target DNA, and a three-nucleotide sequence motif (NGG), known as the PAM, must also be present in the targeted locus (Fig. 4A). Once bound to the target DNA, the Cas9 nuclease introduces a blunt-end DSB three bases upstream of the PAM (Fig. 4A) (Jinek et al., 2012; Cong et al., 2013; Mali et al., 2013). Cas9-induced DSBs are predominantly repaired by the error-prone NHEJ pathway, which results in nonspecific indels (Hsu et al., 2014).

Importantly, however, DSBs can also be repaired by HDR by utilizing exogenous custom repair templates, thus allowing knock-in of specific mutations (Cong et al., 2013). Nevertheless, high editing efficiency requires gRNA targeting close to the intended mutation (Paquet et al., 2016; Liang et al., 2017). Therefore, we focused on the three candidate PAMs identified by CCTop (Stemmer et al., 2015) near the suboptimal/weak TOP2 $\alpha$  E19/I19 5' SS (Fig. 4A). Interestingly, GCD assays demonstrated that only gRNA-2 effectively targeted Cas9 to introduce DSBs in the TOP2 $\alpha$  E19/I19 boundary sequence (Fig. 4, A–C). Given that all three gRNAs anneal with genomic DNA sequences that are in close proximity to each other, differences in accessibility to their TOP2 $\alpha$  E19/I19 boundary targets cannot account for the lack of targeting by gRNA-1 and -3 (Uusi-Mäkelä et al., 2018). It is possible that the lack of gRNA-1 and -3 activity results from either the failure to form a functional Cas9-gRNA complex or internal interactions between the crRNA and tracrRNA that may interfere with Cas9-mediated cleavage (Thyme et al., 2016).

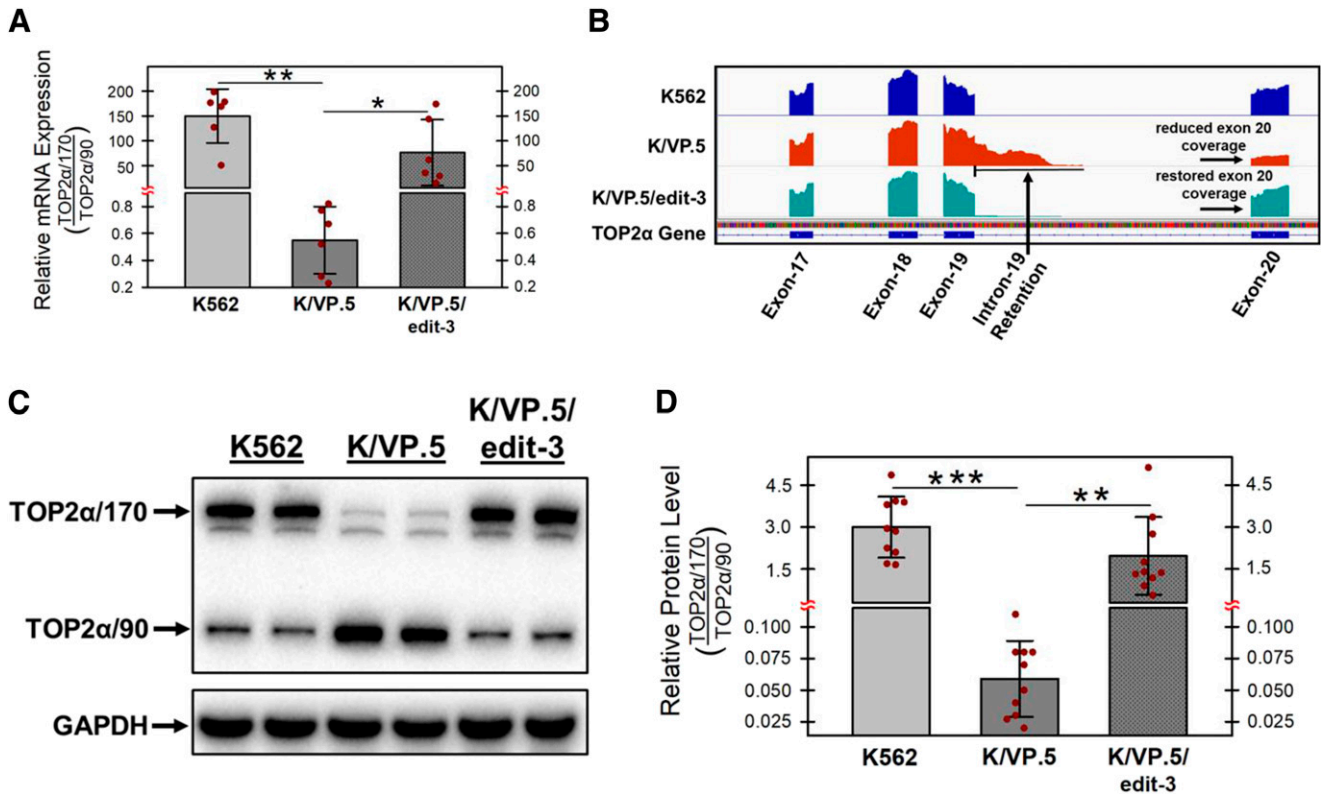


**Fig. 8.** Effects of optimizing the TOP2 $\alpha$  intron 19 5' SS in K/VP.5 on TOP2 $\alpha/170$  mRNA and protein expression in K/VP.5 cells. (A) qPCR analyses were performed from RNA samples isolated from K562, K/VP.5, and KVP.5/edit-3 cells utilizing TaqMan hydrolysis probes specific for TOP2 $\alpha/170$  and TOP2 $\alpha/90$  mRNAs as previously described (Kanagasabai et al., 2017). Results shown are means  $\pm$  S.D. from six cellular RNA isolation experiments performed on separate days;  $P = 0.001$  comparing the difference in mean values for K562 and K/VP.5 mRNAs, 95% CI (93.1, 206.1);  $P = 0.038$  comparing the difference in mean values for K/VP.5/edit-3 vs. K/VP.5 mRNAs, 95% CI (6.4, 145.5). (B) Visualization of retained intron 19 of TOP2 $\alpha$  RNA-seq genome coverage tracks showing the intron 19 retention event in K/VP.5 cells and the restoration of intron removal in K/VP.5/edit-3 cells. Reduced coverage denoted for exon 20 indicates fewer full-length TOP2 $\alpha/170$  reads in K/VP.5 cells. Increased exon 20 coverage in K/VP.5/edit-3 cells indicates restoration of intron 19 removal and more full-length TOP2 $\alpha/170$  reads consistent with expression of greater full-length mature TOP2 $\alpha/170$  mRNA. (C) Representative immunoassay using K562, K/VP.5, and KVP.5/edit-3 cellular lysates. Blots were probed with antibodies specific for the N-terminal portion of TOP2 $\alpha/170/90$  (i.e., amino acids 14–27) or for GAPDH. (D) The ratio of TOP2 $\alpha/170$  to TOP2 $\alpha/90$  protein expression levels was calculated from multiple immunoassays from K562, K/VP.5, and KVP.5/edit-3 cellular lysates. Results shown are means  $\pm$  S.D. from ten experiments performed on separate days;  $P < 0.001$  comparing the difference in mean values for K562 and K/VP.5 cell TOP2 $\alpha/170$  to TOP2 $\alpha/90$  ratios, 95% CI (2.17, 3.71);  $P = 0.002$  comparing the difference in mean values for K/VP.5/edit-3 and K/VP.5 cell TOP2 $\alpha/170$  to TOP2 $\alpha/90$  ratios, 95% CI (0.83, 2.89). \* $P < 0.05$ ; \*\* $P < 0.01$ ; \*\*\* $P < 0.001$ .

To expedite the screening of the edited TOP2 $\alpha$  E19/I19 5' SS in K/VP.5 cells, single-cell clones isolated by limiting dilution were subjected to genomic DNA qPCR utilizing hybridization probes that discriminated between the wild-type TOP2 $\alpha$  E19/I19 and the CRISPR/Cas9-edited TOP2 $\alpha$  E19/I19 boundary (compare Fig. 6, AI and AIV). Of the  $\sim 60$  clonal cell lines screened, nine contained the desired three genomic edits in one TOP2 $\alpha$  allele based on qPCR (Fig. 6AII). Sanger sequencing (Fig. 6BII) from one of the clones was consistent with one TOP2 $\alpha$  allele edited based on the electropherogram peaks with no indication of indels in the two nonedited TOP2 $\alpha$  alleles. Therefore, this clonal cell line (designated K/VP.5/edit-1) was then subjected to an additional round of transfection, and  $\sim 60$  new clonal cell lines were screened by genomic DNA qPCR. Five clones were identified that had the desired edits in two TOP2 $\alpha$  alleles (Fig. 6, AIII and BIII; i.e., K/VP.5/edit-2). One clonal cell line was characterized that had all three TOP2 $\alpha$  alleles properly edited across the TOP2 $\alpha$  E19/I19 5' boundary (Fig. 6, AIV and BIV; i.e., K/VP.5/edit-3). Finally, RsaI restriction enzyme analysis validated the interpretation of the CRISPR/Cas9 editing of TOP2 $\alpha$  alleles in K/VP.5/edit-1–3 clonal cell lines (Fig. 7B).

Characterization of K/VP.5/edit-3 clonal cells revealed that TOP2 $\alpha/90$  protein levels were reduced, whereas TOP2 $\alpha/170$  levels were increased compared with K/VP.5 cells and were at similar levels to those in parental K562 cells (Fig. 8C). In addition, TOP2 $\alpha/170$ :TOP2 $\alpha/90$  mRNA and protein ratios were statistically significantly increased compared with etoposide-resistant K/VP.5 cells and were comparable to the parental K562 cells (Fig. 8, A and D). Together, these results strongly suggested that CRISPR/Cas9 editing of the TOP2 $\alpha$  E19/I19 5' SS improved the removal of I19. RNA-seq genome coverage track reads demonstrated that I19 retention events were decreased in K/VP.5/edit-3 clonal cells compared with K/VP.5 cells (Fig. 8B), thus independently validating our qPCR and Western blot data.

Importantly, functional studies demonstrated that sensitivity to etoposide-induced DNA damage (Fig. 9, A–C) and etoposide-induced growth inhibition (Fig. 10A; Supplemental Table 2; Table 1) was restored in K/VP.5/edit-3 cells to levels comparable to those found in parental K562 cells. The lack of etoposide-induced band depletion for TOP2 $\alpha/90$  in all cell lines (Fig. 9D) is consistent with the absence of the active site Tyr-805 in this truncated isoform, preventing formation of covalent complexes with DNA. Sensitivity to additional TOP2 $\alpha$  poisons

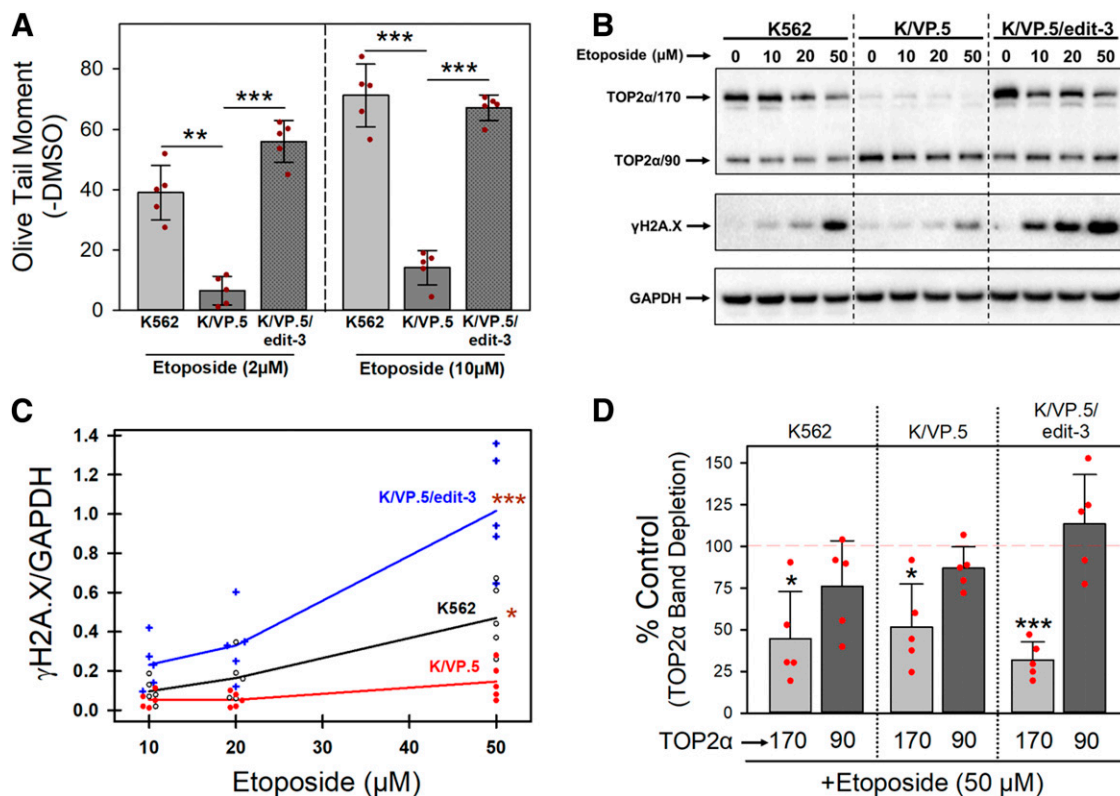


**Fig. 9.** Effects of optimizing the TOP2 $\alpha$  E19/I19 5' SS on sensitivity to etoposide-induced DNA damage. (A) K562, K/VP.5, and KVP.5/edit-3 cells were incubated with etoposide (2 or 10  $\mu$ M) or DMSO (control) for 30 minutes followed by alkaline (pH 13) Comet assays. Results shown are means  $\pm$  S.D. for five cellular experiments run on separate days. For all experimental conditions in each experiment, more than 100 cells were evaluated by OpenComet software. At 2  $\mu$ M etoposide,  $P = 0.005$  comparing the difference in mean values for K562 and K/VP.5 cells, 95% CI (16.8, 48.3);  $P < 0.001$  comparing the difference in mean values for K/VP.5/edit-3 and K/VP.5 cells, 95% CI (39.7, 59.2). At 10  $\mu$ M etoposide,  $P < 0.001$  comparing the difference in mean values for K562 and K/VP.5 cells, 95% CI (41.5, 72.7);  $P < 0.001$  comparing the difference in mean values for K/VP.5/edit-3 and K/VP.5 cells, 95% CI (44.9, 61.1). (B) Representative immunoblot from whole cell lysates of K562, K/VP.5, and K/VP.5/edit-3 cells treated with DMSO or etoposide (10, 20, 50  $\mu$ M) for 30 minutes. The blot was probed with an antibody specific for the N-terminal portion of TOP2 $\alpha$ /170/90 (i.e., amino acids 14–27) and with  $\gamma$ H2A.X and GAPDH antibodies. (C) Scattergram of etoposide-induced DNA double-stranded breaks assessed by  $\gamma$ H2A.X formation. Lines connect the mean values at each etoposide concentration and are derived from five separate cellular experiments performed on separate days under the same conditions as shown in Fig. 9B.  $P = 0.023$  comparing K562 and K/VP.5 cells at 50  $\mu$ M etoposide;  $P < 0.001$  comparing K/VP.5/edit-3 and K/VP.5 cells at 50  $\mu$ M etoposide. Statistical analysis was performed by a repeated measured one-way ANOVA using multiple comparisons vs. the K/VP.5 cell control group (Holm-Sidak method). (D) Etoposide (50  $\mu$ M) induced TOP2 $\alpha$ /170 and TOP2 $\alpha$ /90 band depletion. Results shown are means  $\pm$  S.D. for five separate cellular/immunoblot experiments identical to the representative experiment shown in Fig. 9B. For etoposide-induced TOP2 $\alpha$ /170 band depletion compared with 100% DMSO controls:  $P = 0.012$  K562 cells, 95% CI (20.1, 90.4);  $P = 0.014$  K/VP.5 cells, 95% CI (16.3, 80.3);  $P < 0.001$  K/VP.5/edit-3 cells, 95% CI (54.5, 81.7). For etoposide-induced TOP2 $\alpha$ /90 band depletion compared with 100% controls:  $P = 0.122$  K562 cells;  $P = 0.088$  K/VP.5 cells;  $P = 0.365$  K/VP.5/edit cells. \* $P < 0.05$ ; \*\* $P < 0.01$ ; \*\*\* $P < 0.001$ .

was also completely (e.g., daunorubicin) (Fig. 10B; Table 1) or partially (e.g., mAMSA, mitoxantrone, pixantrone) restored (Fig. 10, C–E; Table 1) in K/VP.5/edit-3 cells.

CRISPR/Cas9 off-target effects might have played a role in the circumvention of the drug resistance phenotype observed in K/VP.5/edit-3 cells (Figs. 9 and 10). To limit mutations (indels) and unwanted chromosomal translocations, we transiently transfected K/VP.5 cells with Cas9/gRNA-2 ribonucleoprotein complexes to restrict the temporal activity of these complexes, improve precision, and reduce off-target effects (Kim et al., 2014). Given that the doubling times for all our cell lines (gene-edited or not) were similar (Supplemental Table 2), CRISPR/Cas9 gene editing did not significantly alter the growth characteristics of K/VP.5 edited cells. In addition, evaluating our RNA-seq data, essential genes (i.e., required for cell survival) (Wang et al., 2019a) were not differentially expressed (fold change cutoff of 2 at 10% false discovery rate) in gene-edited K/VP.5/edit-3 compared with K/VP.5 cells (Supplemental

Fig. 3, denoted in red), consistent with a lack of important off-target effects. Additionally, the CCTop algorithm (Stemmer et al., 2015) was used to predict potential Cas9/gRNA-2 off-target genes where induced DSBs could result in unwanted indels and chromosomal translocations. Given that more than four mismatches between the gRNA and target DNA would prevent Cas9-mediated DSB induction (Cong et al., 2013; Hsu et al., 2013; Cho et al., 2014), potential gRNA-2 off-target sites were predicted, allowing four mismatches and querying the human genomic sequence (*Homo sapiens* GRCh38/hg38). A total of 137 off-target sites were identified. Of these, only 55 were expressed in K/VP.5 and K/VP.5/edit-3 cells. Of the top 20 putative Cas9/gRNA-2 off-target sites/genes, 18 were not differentially expressed (fold change cutoff of 2 at 10% false discovery rate) comparing gene-edited K/VP.5/edit-3 cells and K/VP.5 cells, whereas the two lowest expressing genes in this group exhibited slightly greater than a 2-fold change (Supplemental Fig. 3, denoted in blue), suggesting that off-target effects did not contribute

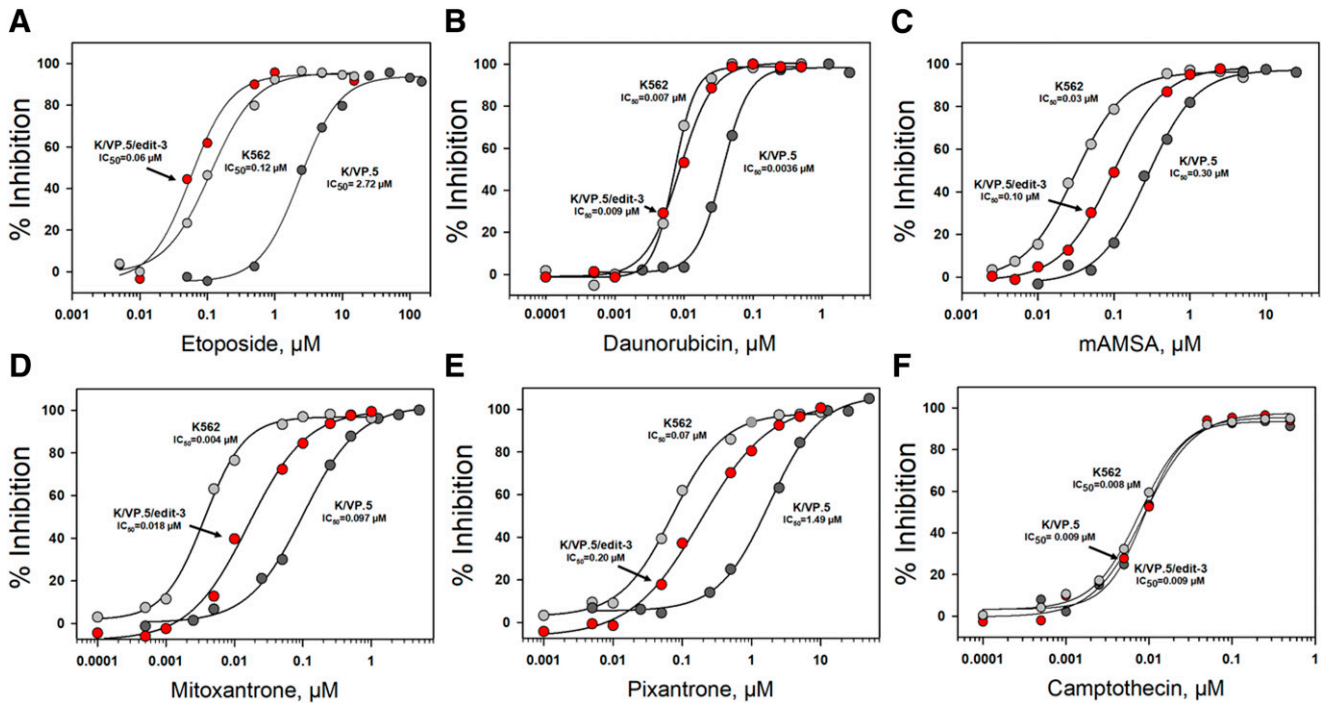


**Fig. 10.** Growth inhibitory effects of etoposide and other topoisomerase-targeted drugs in K562, K/VP.5, and K/VP.5/edit-3 cells. Log-phase cells were incubated for 48 hours with various concentrations of etoposide (A), daunorubicin (B), mAMSA, (C), mitoxantrone (D), pixantrone (E), and camptothecin (F) after which cells were counted on an electronic particle counter (Z1 Coulter counter). The extent of growth beyond the starting concentration in drug-treated vs. DMSO controls was expressed ultimately as percent inhibition. Shown are representative concentration-response (inhibitory) curves for each of the tested drugs with 50% inhibitory concentrations (IC<sub>50</sub> values) indicated. Compilation of replicate experiments performed on different days is shown in Table 1.

to the overall phenotype observed in K/VP.5/edit-3 cells. Of note, the DNA topoisomerase II $\beta$  gene E19/I19 5' SS was one of the top 20 putative Cas9/gRNA-2 off-target sites/genes. To demonstrate that this gene was not targeted by Cas9/gRNA-2, genomic DNA was isolated from K/VP.5/edit-3 cells, and the DNA topoisomerase II $\beta$  E19/I19 boundary was analyzed by a GCD assay; no indels were present (data not shown), suggesting that this gene was not targeted by Cas9/gRNA-2. Finally, circumvention of resistance in K/VP.5/edit-3 cells was observed only to those drugs targeting TOP2 $\alpha$  with no changes in sensitivity to camptothecin, a TOP1 inhibitor, or to podophyllotoxin, a microtubule inhibitor (Table 1). Although CRISPR/Cas9 off-target effects may occur in K/VP.5/edit-3 cells, results suggest that the predominant phenotype

associated with circumvention of resistance appears to be driven by the modifications in the TOP2 $\alpha$  E19/I19 5' SS.

Importantly, the same suboptimal/weak TOP2 $\alpha$  E19/I19 5' SS is present in both parental K562 and resistant K/VP.5 cells (Kanagasabai et al., 2017, 2018). Hence, increased TOP2 $\alpha$  I19 retention in K/VP.5 cells is likely due to aberrant spliceosome function/effectors in this acquired resistant cell line. Our CRISPR/Cas9 editing experiments demonstrated circumvention of resistance by optimizing the TOP2 $\alpha$  E19/I19 5' SS, thereby improving splicing out of I19, decreasing production of TOP2 $\alpha$ /90, and increasing levels of TOP2 $\alpha$ /170 in spite of putative/presumed alterations in spliceosome function. Future studies will focus on the identification and characterization of splicing factors and *cis*-elements regulating

**TABLE 1**  
Growth inhibitory effects of anticancer drugs in K562, K/VP.5, and K/VP.5/edit-3 cells

Anticancer agent	K562 cells (IC <sub>50</sub> ) <sup>a</sup>	K/VP.5 cells (IC <sub>50</sub> )	K/VP.5/edit-3 cells (IC <sub>50</sub> )	Relative resistance <sup>b</sup> (K/VP.5/K562)	Relative resistance <sup>b</sup> (K/VP.5/edit-3/K562)
	nM	nM	nM		
Etoposide	146.8 ± 27.7 (5) <sup>c</sup>	3131 ± 1162 (5)	66.0 ± 6.3 (5)	21.6	0.5
Teniposide	15.5 ± 1.9 (5)	291.2 ± 26.0 (5)	10.1 ± 0.9 (5)	18.8	0.7
Daunorubicin	7.4 ± 0.5 (6)	34.5 ± 3.8 (6)	7.5 ± 1.3 (5)	4.7	1.0
mAMSA	28.8 ± 4.8 (5)	274.0 ± 33.4 (5)	94.0 ± 15.9 (5)	9.6	3.3
Mitoxantrone	3.6 ± 0.6 (5)	104.0 ± 22.1 (5)	14.0 ± 4.0 (5)	29.7	4.0
Pixantrone	81.4 ± 12.1 (5)	1457 ± 227 (5)	233.4 ± 47.7 (5)	18.1	2.9
Camptothecin	11.2 ± 5.0 (5)	10.6 ± 3.5 (5)	10.1 ± 2.7 (5)	0.9	0.9
Podophyllotoxin	10.9 ± 0.4 (3)	10.9 ± 1.3 (3)	10.5 ± 1.1 (3)	1.0	1.0

<sup>a</sup>Fifty percent inhibitory concentration (IC<sub>50</sub>) in a 48-h growth inhibition assay.

<sup>b</sup>IC<sub>50</sub> of K/VP.5 or K/VP.5/edit-3 cells divided by that of the parental K562 cell line.

<sup>c</sup>Mean ± S.D.; numbers in parentheses, number of independent experiments performed on different days.

TOP2 $\alpha$  I19 retention in acquired resistance to TOP2 $\alpha$ -targeting drugs.

#### Acknowledgments

We are grateful to the patients (and healthy volunteers) who provided tissue samples for these studies to The Ohio State University Comprehensive Cancer Center Leukemia Tissue Bank Shared Resource (supported by National Institutes of Health National Cancer Institute P30 CA016058) and to Christopher Manning, Clinical Laboratory Manager, who facilitated our obtaining these samples.

#### Authorship Contributions

*Participated in research design:* Hernandez, Carvajal-Moreno, Papa, Shkolnikov, Ozer, Yalowich, Elton.

*Conducted experiments:* Hernandez, Carvajal-Moreno, Papa, Shkolnikov.

*Contributed new reagents or analytic tools:* Li, Ozer.

*Performed data analysis:* Hernandez, Carvajal-Moreno, Papa, Shkolnikov, Li, Ozer, Yalowich, Elton.

*Wrote or contributed to the writing of the manuscript:* Hernandez, Elton, Yalowich, Li, Ozer.

#### References

- Boutz PL, Bhutkar A, and Sharp PA (2015) Detained introns are a novel, widespread class of post-transcriptionally spliced introns. *Genes Dev* **29**:63–80.
- Capelôa T, Benyahia Z, Zampieri LX, Blackman MCN, and Sonveaux P (2020) Metabolic and non-metabolic pathways that control cancer resistance to anthracyclines. *Semin Cell Dev Biol* **98**:181–191.
- Chen SH, Chan NL, and Hsieh TS (2013) New mechanistic and functional insights into DNA topoisomerases. *Annu Rev Biochem* **82**:139–170.
- Cho SW, Kim S, Kim Y, Kweon J, Kim HS, Bae S, and Kim JS (2014) Analysis of off-target effects of CRISPR/Cas-derived RNA-guided endonucleases and nickases. *Genome Res* **24**:132–141.
- Cioe L, McNab A, Hubbell HR, Meo P, Curtis P, and Rovera G (1981) Differential expression of the globin genes in human leukemia K562(S) cells induced to differentiate by hemin or butyric acid. *Cancer Res* **41**:237–243.
- Cong L, Ran FA, Cox D, Lin S, Barretto R, Habib N, Hsu PD, Wu X, Jiang W, Marraffini LA, et al. (2013) Multiplex genome engineering using CRISPR/Cas systems. *Science* **339**:819–823.
- Cooper TA (2005) Use of minigene systems to dissect alternative splicing elements. *Methods* **37**:331–340.
- Deweese JE and Osheroff N (2009) The DNA cleavage reaction of topoisomerase II: wolf in sheep's clothing. *Nucleic Acids Res* **37**:738–748.
- Eckert D, Andr e N, Razanau A, Zock-Emmenthal S, L utzelberger M, Plath S, Schmidt H, Guerra-Moreno A, Cozzuto L, Ayt e J, et al. (2016) Prp4 kinase grants the license to splice: control of weak splice sites during spliceosome activation. *PLoS Genet* **12**:e1005768.
- Elton TS, Ozer HG, and Yalowich JC (2020) Effects of DNA topoisomerase II $\alpha$  splice variants on acquired drug resistance. *Cancer Drug Resist* **3**:161–170.
- Gadepalli VS, Ozer HG, Yilmaz AS, Pietrzak M, and Webb A (2019) BISR-RNAseq: an efficient and scalable RNAseq analysis workflow with interactive report generation. *BMC Bioinformatics* **20** (Suppl 24):670.
- Ganapathi RN and Ganapathi MK (2013) Mechanisms regulating resistance to inhibitors of topoisomerase II. *Front Pharmacol* **4**:89.
- Gyori BM, Venkatachalam G, Thiagarajan PS, Hsu D, and Clement MV (2014) OpenComet: an automated tool for comet assay image analysis. *Redox Biol* **2**:457–465.
- Harker WG, Slade DL, Parr RL, and Holguin MH (1995) Selective use of an alternative stop codon and polyadenylation signal within intron sequences leads to a truncated topoisomerase II alpha messenger RNA and protein in human HL-60 leukemia cells selected for resistance to mitoxantrone. *Cancer Res* **55**:4962–4971.
- Hicks MJ, Mueller WF, Shepard PJ, and Hertel KJ (2010) Competing upstream 5' splice sites enhance the rate of proximal splicing. *Mol Cell Biol* **30**:1878–1886.
- Hsu PD, Scott DA, Weinstein JA, Ran FA, Konermann S, Agarwala V, Li Y, Fine EJ, Wu X, Shalem O, et al. (2013) DNA targeting specificity of RNA-guided Cas9 nucleases. *Nat Biotechnol* **31**:827–832.
- Hsu PD, Lander ES, and Zhang F (2014) Development and applications of CRISPR-Cas9 for genome engineering. *Cell* **157**:1262–1278.
- Huang SC, Ou AC, Park J, Yu F, Yu B, Lee A, Yang G, Zhou A, and Benz EJ Jr (2012) RFXO2 promotes protein 4.1R exon 16 selection via U1 snRNP recruitment. *Mol Cell Biol* **32**:513–526.
- Jinek M, Chylinski K, Fonfara I, Hauer M, Doudna JA, and Charpentier E (2012) A programmable dual-RNA-guided DNA endonuclease in adaptive bacterial immunity. *Science* **337**:816–821.
- Kanagasabai R, Karmahapatra S, Kientz CA, Yu Y, Hernandez VA, Kania EE, Yalowich JC, and Elton TS (2018) The novel C-terminal truncated 90-kDa isoform of topoisomerase II $\alpha$  (TOP2 $\alpha$ /90) is a determinant of etoposide resistance in K562 leukemia cells via heterodimerization with the TOP2 $\alpha$ /170 isoform. *Mol Pharmacol* **93**:515–525.
- Kanagasabai R, Serdar L, Karmahapatra S, Kientz CA, Ellis J, Ritke MK, Elton TS, and Yalowich JC (2017) Alternative RNA processing of topoisomerase II $\alpha$  in etoposide-resistant human leukemia K562 cells: intron retention results in a novel C-terminal truncated 90-kDa isoform. *J Pharmacol Exp Ther* **360**:152–163.
- Kaufmann SH and Svingen PA (1999) Immunoblot analysis and band depletion assays. *Methods Mol Biol* **94**:253–268.
- Kim D, Langmead B, and Salzberg SL (2015) HISAT: a fast spliced aligner with low memory requirements. *Nat Methods* **12**:357–360.
- Kim S, Kim D, Cho SW, Kim J, and Kim JS (2014) Highly efficient RNA-guided genome editing in human cells via delivery of purified Cas9 ribonucleoproteins. *Genome Res* **24**:1012–1019.
- Kurosaki T and Maquat LE (2016) Nonsense-mediated mRNA decay in humans at a glance. *J Cell Sci* **129**:461–467.
- Labuhn M, Adams FF, Ng M, Knoess S, Schambach A, Charpentier EM, Schwarzer A, Mateo JL, Klusmann JH, and Heckl D (2018) Refined sgRNA efficacy prediction improves large- and small-scale CRISPR-Cas9 applications. *Nucleic Acids Res* **46**:1375–1385.
- Lee Y and Rio DC (2015) Mechanisms and regulation of alternative pre-mRNA splicing. *Annu Rev Biochem* **84**:291–323.
- Li Y, Bor YC, Fitzgerald MP, Lee KS, Rekosh D, and Hammarskjold ML (2016) An NXF1 mRNA with a retained intron is expressed in hippocampal and neocortical neurons and is translated into a protein that functions as an Nxf1 cofactor. *Mol Biol Cell* **27**:3903–3912.
- Liang X, Potter J, Kumar S, Ravinder N, and Chesnut JD (2017) Enhanced CRISPR/Cas9-mediated precise genome editing by improved design and delivery of gRNA, Cas9 nuclease, and donor DNA. *J Biotechnol* **241**:136–146.
- Liao Y, Smyth GK, and Shi W (2014) featureCounts: an efficient general purpose program for assigning sequence reads to genomic features. *Bioinformatics* **30**:923–930.
- Luke AM, Chastain PD, Pachkowski BF, Afonin V, Takeda S, Kaufman DG, Swenberg JA, and Nakamura J (2010) Accumulation of true single strand breaks and AP sites in base excision repair deficient cells. *Mutat Res* **694**:65–71.
- Mali P, Yang L, Esvelt KM, Aach J, Guell M, DiCarlo JE, Norville JE, and Church GM (2013) RNA-guided human genome engineering via Cas9. *Science* **339**:823–826.
- Middleton R, Gao D, Thomas A, Singh B, Au A, Wong JJ, Bomane A, Cosson B, Eyras E, Rasko JEJ, et al. (2017) IRFinder: assessing the impact of intron retention on mammalian gene expression. *Genome Biol* **18**:51.
- Mo YY and Beck WT (1997) Heterogeneous expression of DNA topoisomerase II alpha isoforms in tumor cell lines. *Oncol Res* **9**:193–204.
- Monteuuis G, Wong JLL, Bailey CG, Schmitz U, and Rasko JEJ (2019) The changing paradigm of intron retention: regulation, ramifications and recipes. *Nucleic Acids Res* **47**:11497–11513.
- Nitiss JL (2009) Targeting DNA topoisomerase II in cancer chemotherapy. *Nat Rev Cancer* **9**:338–350.
- Olive PL (2002) The comet assay. An overview of techniques. *Methods Mol Biol* **203**:179–194.
- Paquet D, Kwart D, Chen A, Sproul A, Jacob S, Teo S, Olsen KM, Gregg A, Nogge S, and Tessier-Lavigne M (2016) Efficient introduction of specific homozygous and heterozygous mutations using CRISPR/Cas9. *Nature* **533**:125–129.
- Pommier Y and Marchand C (2011) Interfacial inhibitors: targeting macromolecular complexes. *Nat Rev Drug Discov* **11**:25–36.
- Pommier Y, Sun Y, Huang SN, and Nitiss JL (2016) Roles of eukaryotic topoisomerases in transcription, replication and genomic stability. *Nat Rev Mol Cell Biol* **17**:703–721.
- Qi LS, Larson MH, Gilbert LA, Doudna JA, Weissman JS, Arkin AP, and Lim WA (2013) Repurposing CRISPR as an RNA-guided platform for sequence-specific control of gene expression. *Cell* **152**:1173–1183.
- Ramirez F, Ryan DP, Gruning B, Bhardwaj V, Kilpert F, Richter AS, Heyne S, D undar F, and Manke T (2016) deepTools2: a next generation web server for deep-sequence data analysis. *Nucleic Acids Res* **44**:W160–W165.
- Ritchie ME, Phipson B, Wu D, Hu Y, Law CW, Shi W, and Smyth GK (2015) Limma powers differential expression analyses for RNA-sequencing and microarray studies. *Nucleic Acids Res* **43**:e47.
- Ritke MK and Yalowich JC (1993) Altered gene expression in human leukemia K562 cells selected for resistance to etoposide. *Biochem Pharmacol* **46**:2007–2020.
- Ritke MK, Roberts D, Allan WP, Raymond J, Bergoltz VV, and Yalowich JC (1994) Altered stability of etoposide-induced topoisomerase II-DNA complexes in resistant human leukemia K562 cells. *Br J Cancer* **69**:687–697.
- Robinson JT, Thorvaldsd ottir H, Winckler W, Guttman M, Lander ES, Getz G, and Mesirov JP (2011) Integrative genomics viewer. *Nat Biotechnol* **29**:24–26.
- Rogakou EP, Pilch DR, Orr AH, Ivanova VS, and Bonner WM (1998) DNA double-stranded breaks induce histone H2AX phosphorylation on serine 139. *J Biol Chem* **273**:5858–5868.
- Schmittgen TD and Livak KJ (2008) Analyzing real-time PCR data by the comparative  $C_T$  method. *Nat Protoc* **3**:1101–1108.
- Shoubridge C, Jackson M, Grinton B, Berkovic SF, Scheffer IE, Huskins S, Thomas A, and Ware T (2019) Splice variant in ARX leading to loss of C-terminal region in a boy with intellectual disability and infantile onset developmental and epileptic encephalopathy. *Am J Med Genet A* **179**:1483–1490.
- Stemmer M, Thumberger T, Del Sol Keyer M, Wittbrodt J, and Mateo JL (2015) CCTop: an intuitive, flexible and reliable CRISPR/Cas9 target prediction tool. *PLoS One* **10**:e0124633.
- Thyme SB, Akhmetova L, Montague TG, Valen E, and Schier AF (2016) Internal guide RNA interactions interfere with Cas9-mediated cleavage. *Nat Commun* **7**:11750.
- Uusi-M akel a MIE, Barker HR, B auerlein CA, H akkinen T, Nykter M, and R amet M (2018) Chromatin accessibility is associated with CRISPR-Cas9 efficiency in the zebrafish (*Danio rerio*). *PLoS One* **13**:e0196238.
- Uzor S, Zorzou P, Bowler E, Porazinski S, Wilson I, and Ladomery M (2018) Autoregulation of the human splice factor kinase CLK1 through exon skipping and intron retention. *Gene* **670**:46–54.

- Vlasova II, Feng WH, Goff JP, Giorgianni A, Do D, Gollin SM, Lewis DW, Kagan VE, and Yalowich JC (2011) Myeloperoxidase-dependent oxidation of etoposide in human myeloid progenitor CD34+ cells. *Mol Pharmacol* **79**:479–487.
- Wang B, Wang M, Zhang W, Xiao T, Chen CH, Wu A, Wu F, Traugh N, Wang X, Li Z, et al. (2019) Integrative analysis of pooled CRISPR genetic screens using MAGeCKFlute. *Nat Protoc* **14**:756–780.
- Wang C and Buolamwini JK (2019) A novel RNA variant of human concentrative nucleoside transporter 1 (hCNT1) that is a potential cancer biomarker. *Exp Hematol Oncol* **8**:18.
- Wickramasinghe VO, González-Porta M, Perera D, Bartolozzi AR, Sibley CR, Hallegger M, Ule J, Marioni JC, and Venkitaraman AR (2015) Regulation of constitutive and alternative mRNA splicing across the human transcriptome by PRPF8 is determined by 5' splice site strength. *Genome Biol* **16**:201.
- Yu Q, Mirski SE, Sparks KE, and Cole SP (1997) Two COOH-terminal truncated cytoplasmic forms of topoisomerase II  $\alpha$  in a VP-16-selected lung cancer cell line result from partial gene deletion and alternative splicing. *Biochemistry* **36**:5868–5877.
- Yue M and Ogawa Y (2018) CRISPR/Cas9-mediated modulation of splicing efficiency reveals short splicing isoform of Xist RNA is sufficient to induce X-chromosome inactivation. *Nucleic Acids Res* **46**:e26.
- Zhou B, Ho SS, Greer SU, Zhu X, Bell JM, Arthur JG, Spies N, Zhang X, Byeon S, Pattni R, et al. (2019) Comprehensive, integrated, and phased whole-genome analysis of the primary ENCODE cell line K562. *Genome Res* **29**:472–484.

---

**Address correspondence to:** Jack C. Yalowich, Division of Pharmaceutics and Pharmacology, College of Pharmacy, The Ohio State University, 500 West 12th Ave., Columbus, OH 43210. E-mail: yalowich.1@osu.edu; or Terry S. Elton, Division of Pharmaceutics and Pharmacology, College of Pharmacy, The Ohio State University, 500 West 12th Ave., Columbus, OH 43210. E-mail: elton.8@osu.edu

---